UNIVERSITY OF ILLINOIS
URBANA

AERONOMY REPORT NO. 59

COLLECTION AND PROCESSING OF DATA FROM A PHASE-COHERENT METEOR RADAR

by
C. A. Backof, Jr.
S. A. Bowhill

April 1, 1974

Supported by
National Aeronautics and Space Administration
Grant NGR-14-005-181

Aeronomy Laboratory
Department of Electrical Engineering
University of Illinois
Urbana, Illinois

UILU-Eng-74-2502

A E R O N O M Y R E P O R T

N O. 59

COLLECTION AND PROCESSING OF DATA FROM A PHASE-COHERENT METEOR RADAR

by

C. A. Backof, Jr.
S. A. Bowhill

April 1, 1974

Supported by
National Aeronautics
and Space Administration
NGR-14-005-181

Aeronomy Laboratory
Department of Electrical Engineering
University of Illinois
Urbana, Illinois

ABSTRACT

An analysis of the measurement accuracy requirements of a high-resolution meteor radar for observing short-period atmospheric waves is presented, and a system which satisfies the requirements is described. A medium-scale, real-time computer is programmed to perform all echo-recognition and coordinate-measurement functions. The measurement algorithms are exercised on noisy data generated by a program which simulates the hardware system, in order to find the effects of noise on the measurement accuracies. Under typical conditions, the height accuracy is ±1 km, and the velocity accuracy ±5 $msec^{-1}$; these accuracies are sufficient for the study of the structure of atmospheric winds in the 80-120 km height region.

TABLE OF CONTENTS

Page

LIST OF TABLES

LIST OF FIGURES

Figure Page

1. INTRODUCTION

1.1 *Winds in the Upper Atmosphere*

The neutral winds in the atmosphere can be decomposed into three components: prevailing wind, tidal wind, and irregular wind [*Beer*, 1972]. The prevailing wind is predominantly east-west. This east-west flow varies through the course of the year in a characteristic pattern in both hemispheres according to season. Diurnal periodic motions due to atmospheric tides are superimposed on these prevailing winds. Tides are most visible in wind studies at 85-105 km [*Greenhaw and Neufeld*, 1956]. Tidal theory predicts that the amplitude of these waves should increase upwards as $\rho^{-1/2}$, where the neutral gas density ρ decreases almost exponentially in the atmosphere. This increase in amplitude is a direct consequence of conservation of energy. If A is the amplitude of an atmopsheric tidal wave, then the kinetic energy is given by $\rho A^2/2$, which must remain constant in the absence of dissipative forces.

Since the atmosphere is stratified by a gravitational field, there exists a class of waves in which the air particle motions are transverse relative to the direction of propagation of the wave. When the effects of gravity and density stratification become dominant, atmospheric gravity waves result. These atmospheric gravity waves are so named because their behavior is influenced by gravitational forces. Such waves have interested meteorologists for quite a long time [*Haurwitz*, 1951]. Observation of winds reveals a scattering of velocities about the regular oscillations of the tidal wind. This irregular wind makes the largest contribution to the total wind vector, and increases in amplitude with height, just as tidal waves do. *Hines* [1960] showed that these apparently random variations could

be explained in terms of internal gravity waves. *Greenhow and Neufeld* [1959] found that the irregular winds in their 1956 data had a time scale of about 100 minutes and vertical scale of about 6 km. Photographs of long-enduring meteor trails provide a more direct measurement of the vertical scale of the irregular winds. These trails are rapidly distorted from their initial straight-line shape. In recent years, most of the information about vertical structure of the irregular winds has come from chemical trails released by rocket experiments. Observation of these trails indicate unambiguously that the irregular winds are predominantly horizontal, with amplitudes increasing with height.

Much of the irregular motion in the ionosphere was at one time thought to be turbulence. Turbulence power estimates (i.e., the rate of dissipation of turbulence energy) were as high as 25 watts per kilogram [*Booker*, 1956]; such high estimates were based on motions now attributed to gravity waves. Turbulence is much weaker than was previously believed, but is nonetheless present at heights up to 100 km [*Hines*, 1963].

Turbulence is obvious from the diffusive growth of meteor trails. The trail cross section increases first because of molecular diffusion, but in a few seconds eddy diffusion gains importance and ultimately dominates. *Greenhow* [1959] has deduced from this transitional growth that a turbulent power of 7×10^{-3} watts per kilogram is present at meteor heights.

With this value for turbulent power, *Hines* [1963] attempted to get some idea of the scale of the turbulent spectrum [*Booker*, 1956]. Values for the length scale L_2, time scale T_2, and velocity V_2 of the small scale

end of the spectrum can be calculated once the kinematic viscosity factor is known. This factor is approximately 10 $m^2 sec^{-1}$ at 95 km [*Minzner, et al.*, 1959]. The values were calculated, yielding

$$L_2 \cong 20 \text{ m}$$
$$T_2 \cong 40 \text{ sec}$$
$$V_2 \cong .5 \text{ msec}^{-1}$$

This scale of L_2 is comparable to the scale observed by *Blamont and Jager* [1961], and is also compatible with the scale of ionization irregularities that are observed by the scattering of radio waves [*Bowles*, 1959]. It is important to note that, in fact, the scale of turbulence is not a constant. The corresponding values for the large-scale end of the spectrum (L_1, T_1, V_1) are not uniquely specified. They are, however, limited by the processes which generate the turbulence. These processes are generally believed to be associated with the irregular wind. *Hines* [1963] chose $T_1 < 1000$ sec, and then calculated $V_1 < 3 \text{msec}^{-1}$ and $L_1 < 3000$ m.

These various estimates are based on the application of standard turbulence formulas. Since these formulas are derived for incompressible fluids, and ignore anisotropies present in a stratified fluid such as the ionosphere, they can be taken as conditionally acceptable relationships which may or may not be verified through further study.

1.2 *Measurement Techniques*

Wind measurements above 80 km fall into two general categories: those in which the experimenter places a probe or tracer in the atmosphere; and those in which the experimenter relies on some natural phenomenon to act

as a tracer. In the first category, several techniques are available, among which are grenades, Pitot tubes, falling spheres, and chemical releases. Each of these techniques uses a fairly large rocket to carry the experiment to the required height, and each returns usable data for a rather short period, ranging from a few minutes to an hour. All of these rocket techniques are expensive, and limited by the short measurement interval.

Several natural phenomena are useful for atmospheric wind measurement. Observation of noctilucent clouds is one of the oldest wind measurement techniques [*Witt*, 1962]. Noctilucent cloud occurrence is unpredictable, however, and limited to twilight hours. For these reasons, the method is not useful for systematic wind studies. *Mitra* [1949] is responsible for a technique which tracks the movement of ionospheric irregularities by ground-based radio measurement. This method is, however, subject to difficulty in interpretation of fading records.

Observation of meteor trails is another wind determination method. *Manning et. al.* [1950] showed that meteor trails move with the surrounding atmosphere, and are therefore, useful in wind studies. Visible meteor trails occur rather infrequently, but ground-based radar systems can detect the invisible but much more frequent trails left by meteors smaller than a grain of sand. Since meteors enter the atmosphere throughout the day, a nearly continuous sampling of atmospheric wind is available from the method.

Ionospheric motions have also been observed using partial reflection systems with spaced receivers. The velocity of a diffraction pattern formed on the ground by radio waves partially reflected from the 60-100 km region

is measured by comparing signals received at separated antennas. Meteor radar, however, is a more common measurement technique, and the technique with the most potential for continuous wind study.

1.2.1 *Meteor-radar technique.* A meteor entering the atmosphere is heated by frictional forces. The high temperature of the meteor causes ionization of the atmosphere it is passing through, and also causes self-vaporization. The ionized molecules from the atmosphere and the meter itself form a trail in the wake of the meteor. This ionized trail is a good specular reflector for VHF radio waves; that is, VHF waves are reflected from the trails, with the angle of incidence equalling the angle of reflection. A radio wave is reflected back toward its source if the meteor trail is oriented perpendicular to the direction of propagation of the wave.

Meteor trails move with the surrounding atmosphere, causing a Doppler frequency shift in the reflected wave. For a pulse transmitted at a frequency f_t, reflected from a target moving with velocity v relative to the radio source, the received signal f_r is given by the expression

$$f_r = \frac{1 + v/c}{1 - v/c} f_t \tag{1.1}$$

where c is the velocity of propagation of the radio wave. For the condition v much less than c, the received signal f_r may be approximated

$$f_r \cong \left(1 + \frac{2v}{c}\right) f_t \quad . \tag{1.2}$$

Wind velocities in the atmosphere are certainly much less than the speed of light, so that the approximation is valid. The Doppler frequency shift of the returned signal is

$$\Delta f = \frac{2v}{c} f_t \tag{1.3}$$

Once formed, meteor trails grow in size through diffusion. As the trails grow, reflected signal initially increases in strength and then decreases to zero as the trail is dissipated.

The majority of meteor-radar stations measure nothing more than the Doppler shifts of meteor trail echoes. Since meteor trails occur in the height region from 80 - 120 km, such systems measure an average wind. This average is weighted, however, because most returns come from about 95 km. More elaborate systems measure the angles of arrival and range of the reflection point in addition to the Doppler shift. With this information, the height of the reflection can be calculated, and a wind profile of the 80 - 120 km region can be developed.

Other schemes for measuring height have been used. One technique is to observe the rate of decay of the received signal amplitude. Since the atmospheric density decreases with height, meteor trails at higher heights diffuse faster than those at lower heights. This method can yield reflection heights to within ±2 km at best [*Lee and Geller* 1973].

1.2.2 *Limitations of previous systems.* Existing meteor-radar experiments have a number of limitations. Because of uncertainties in height measurement, wind shears and sharp wind velocity gradients are smoothed by spatial averaging, and cannot be accurately measured. Also, long delays occur between the collection of raw data and the development of wind profiles. These delays are due to the fact that collection occurs

at one place, and processing at another; in addition, processing has traditionally involved many manual operations. For these reasons, experimental programs which use the results of one experiment to plan another are severely limited.

The rate of meteor trail echoes has also been a limiting factor. The observation of gravity waves requires that hundreds of meteor trails per hour be recorded, while current systems can provide only tens of trails per hour [*Barnes*, 1968]. Another requirement for gravity wave observation is height accuracy greater than 1 km. Such accuracy has not yet been achieved.

1.2.3 *Advantages of the proposed system.* The Illinois meteor-radar system has a number of advantages over other systems. Height uncertainty is reduced to ±1 km by improvements in elevation angle and range measurement schemes. A medium-scale computer is included as an integral part of the system so that the velocities and polar coordinates of specular reflection points can be determined in real time. Much of the measurement and control hardware has been replaced by programmed algorithms, bringing improvements in overall system reliability and flexibility. Lastly, the system transmitter has a power output of 5 Mw, which is about two orders of magnitude more power than other meteor-radar systems used. This high power will yield about one order of magnitude more meteor trail echoes per unit time than other systems.

1.3 *Statement of the Problem*

The research reported on in this thesis covers four areas:

1) Specification of free parameters such as transmitter pulse repetition frequency (PRF), pulse width and shape, and receiver bandwidth.

2) Design of a software system for the collection and processing of data, and allocation of the computer attributes to the tasks involved.
3) Design of the required measurement algorithms.
4) Demonstration of the data reduction routines through computer simulation of the hardware system and collection software.

Design decisions made in any one of the first three areas has a direct impact on the other two. The role of the fourth area of effort is to analyze the total effect of any decision relating to the first three areas. The over-all effort of this research, therefore, is to recognize the tradeoffs involved in each design decision, and maximize the usable data output of the system, subject to the accuracy and hardware constraints.

1.4 *Outline of Thesis*

The remainder of this thesis is organized as follows. Section 2 describes the atmospheric phenomena to be observed, and gives the system constraints required to measure the phenomena, such as measurement accuracy and required echo rate. Also, the constraints set by the system which were pre-defined. These system features are the given, around which other aspects must be planned. Section 3.2 is the beginning of the description of the system design effort. Sections 3.3 and 3.4 detail the software data organization, and outline the levels of processing involved. The logical flow of software control is also given. Section 4 describes each of the required routines. In addition, the effect of quantization and sky noise on algorithm accuracy, and the impact of hardware parameter selection (e.g. PRF, pulse width) on data reduction, is examined. Section 5 presents the system capabilities and signal-to-noise

ratio requirements. Section 6 gives a summary of all work done, and presents some ideas for future efforts. In particular, a re-evaluation of the software-hardware tradeoffs is made, and a proposal for the addition of some external control hardware to the system is given.

2. SCIENTIFIC CRITERIA AND SPECIFICATIONS

2.1 *Scientific Objectives*

The objective of the Illinois meteor-radar program is to build a system that is compatible with nationally and internationally coordinated meteor wind programs, and also with specific research efforts where a single station is of value. Some of the observational programs requiring a coordinated network are investigation of planetary wave propagation into the lower thermosphere, investigation of winter changes in mesospheric and lower thermospheric circulation, observational studies of the latitudinal structure of tides, and studies of the geographic variation in atmospheric turbulence. Observational programs of scientific interest for a single station include studies of diurnal and seasonal variation of turbulence, comparison of thermospheric circulation and solar activity, and observation of the small-scale wind structure.

Figures 2.1 and 2.2 [*Rosenberg*, 1968] show the north-south and east-west components of a collection of 60 wind profiles measured by observation of chemical releases from rockets. Rosenberg resolved the data shown in these two figures into total wind speed shown in Figure 2.3, and wind shear, shown in Figure 2.4. The most that could possibly be expected of a meteor radar system is that it produce measured wind profiles comparable to those from rocket releases.

Rosenberg and Zimmerman [1972] studied the shear-related properties of winds in the meteor region. Table 2.1 contains some of their results. From these data, measurement criteria for the meteor-radar system were developed. It is desirable to build a system that can:

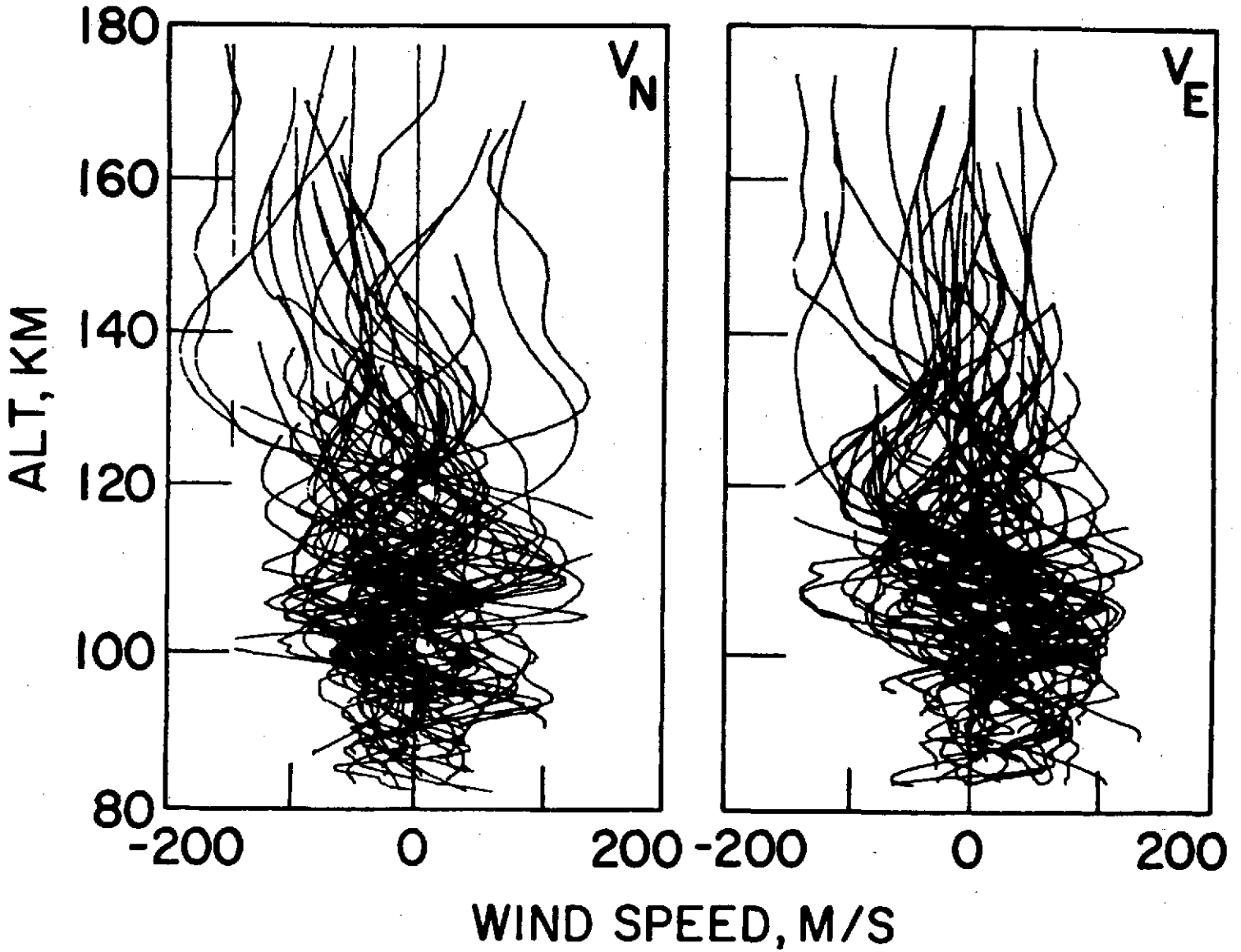

Figure 2.1

Figure 2.2

Wind component velocity versus altitude from [*Rosenberg*, 1968].

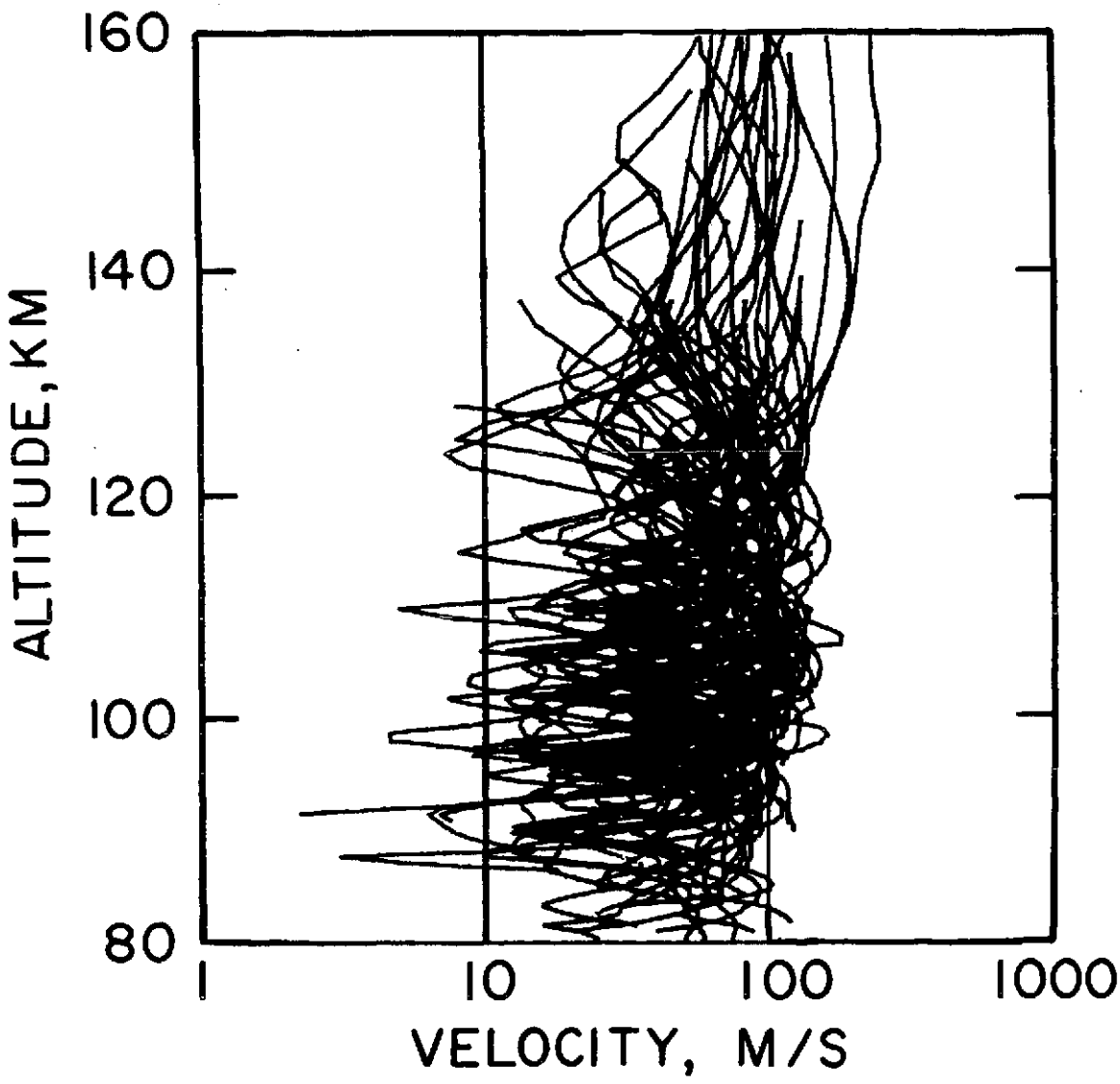

Figure 2.3. Total wind speed versus altitude from [*Rosenberg*, 1968].

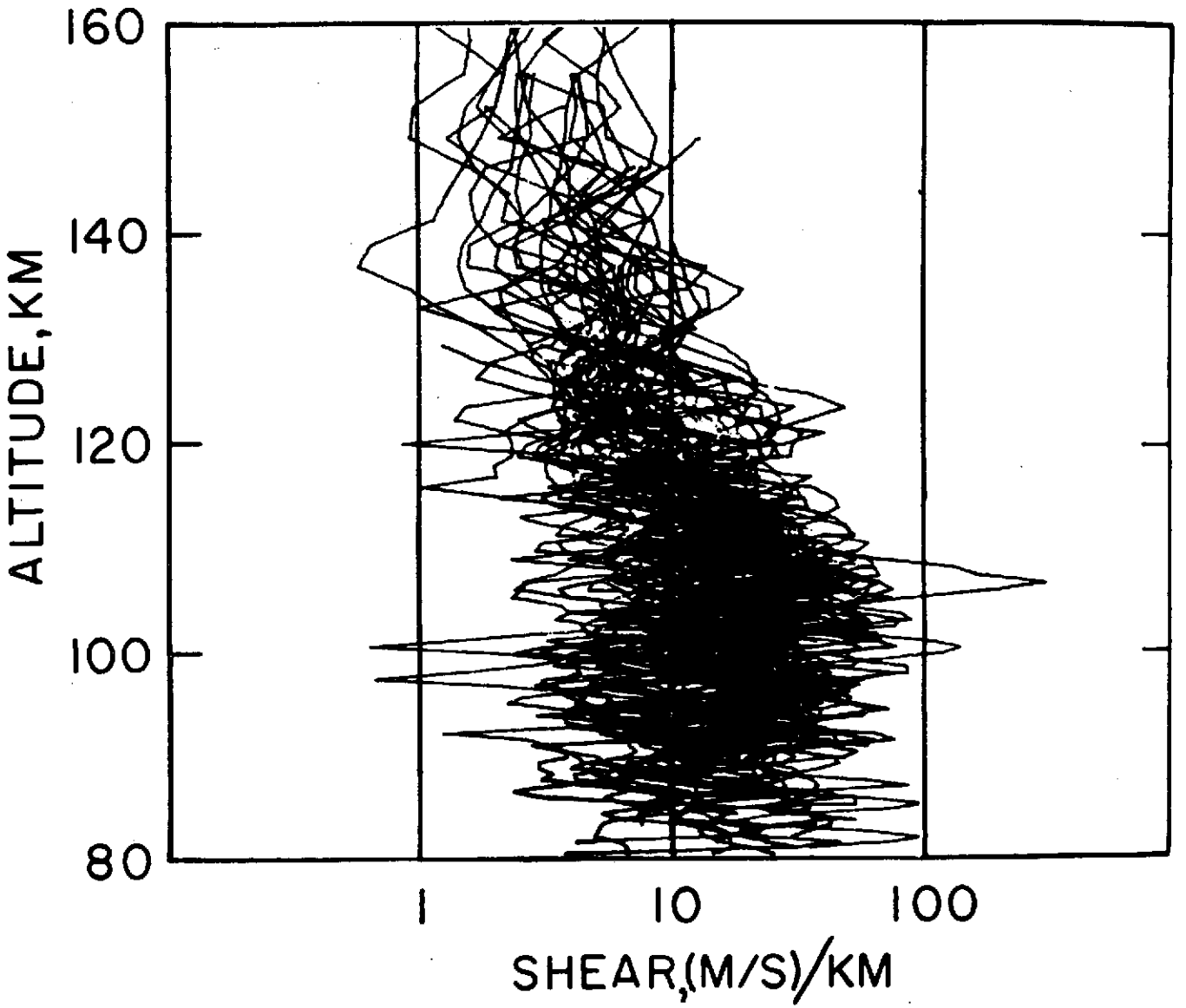

Figure 2.4. Wind shear, m/sec/km versus altitude from [*Rosenberg*, 1968].

Table 2.1

Shear-related properties of winds in the 90-120 km region

1. Altitude, km	90-97	97-103	103-110	110-120
2. Total samples	101	534	764	482
3. Mean velocity, ms^{-1}	48	58	60	64
4. Wave amplitude, ms^{-1}	35	45	48	52
5. $Shear_{lim}$, ms^{-1} km^{-1}	75	75	75	50
6. $Shear_{avg}$, ms^{-1} km^{-1}	21	21	21	14
7. $Shear_{rms}$, ms^{-1} km^{-1}	27	27	27	18
8. $Wavelength_{mean}$, km	14	16	18	24
9. $Wavelength_{lim}$, km	3.5	4.0	4.5	6.0

1) Measure winds in excess of 100 $msec^{-1}$, with accuracy a small fraction, of typical atmospheric wave amplitudes.
2) Resolve shears on the order of 50 $msec^{-1}$ km^{-1}.
3) Measure height, with accuracy a small fraction of the vertical dimension of the atmospheric waves of interest.

There are other requirements for the longer period dynamics. These include measurement of two horizontal components, and the capability for extended operation.

2.2. *Number of Meteors Per Hour*

The shortest period oscillation that can be observed by a meteor radar is determined by the meteor echo rate. The Brunt-Vaisala frequency, ω_g, is the highest frequency wave that can exist in an isothermal atmosphere. This frequency is given by the relation

$$\omega_g = (\gamma-1)^{1/2}\, g/C \qquad (2.1)$$

$$\gamma = \frac{C_p}{C_v} = 1.4$$

$g = 9.8\ msec^{-2}$

C = speed of sound

Figure 2.5 adapted from *Georges* [1967] shows that the period $(2\pi/\omega_g)$ of the Brunt-Vaisala frequency in the 80-120 km region is about 5 min. Observation of this frequency requires at least one return per min from any given height. If meteor echoes were uniformly distributed over the 80-120 km region, observation of this wave structure with one km height accuracy would require 40 echoes per min, or 2400 per hr. Meteor echoes

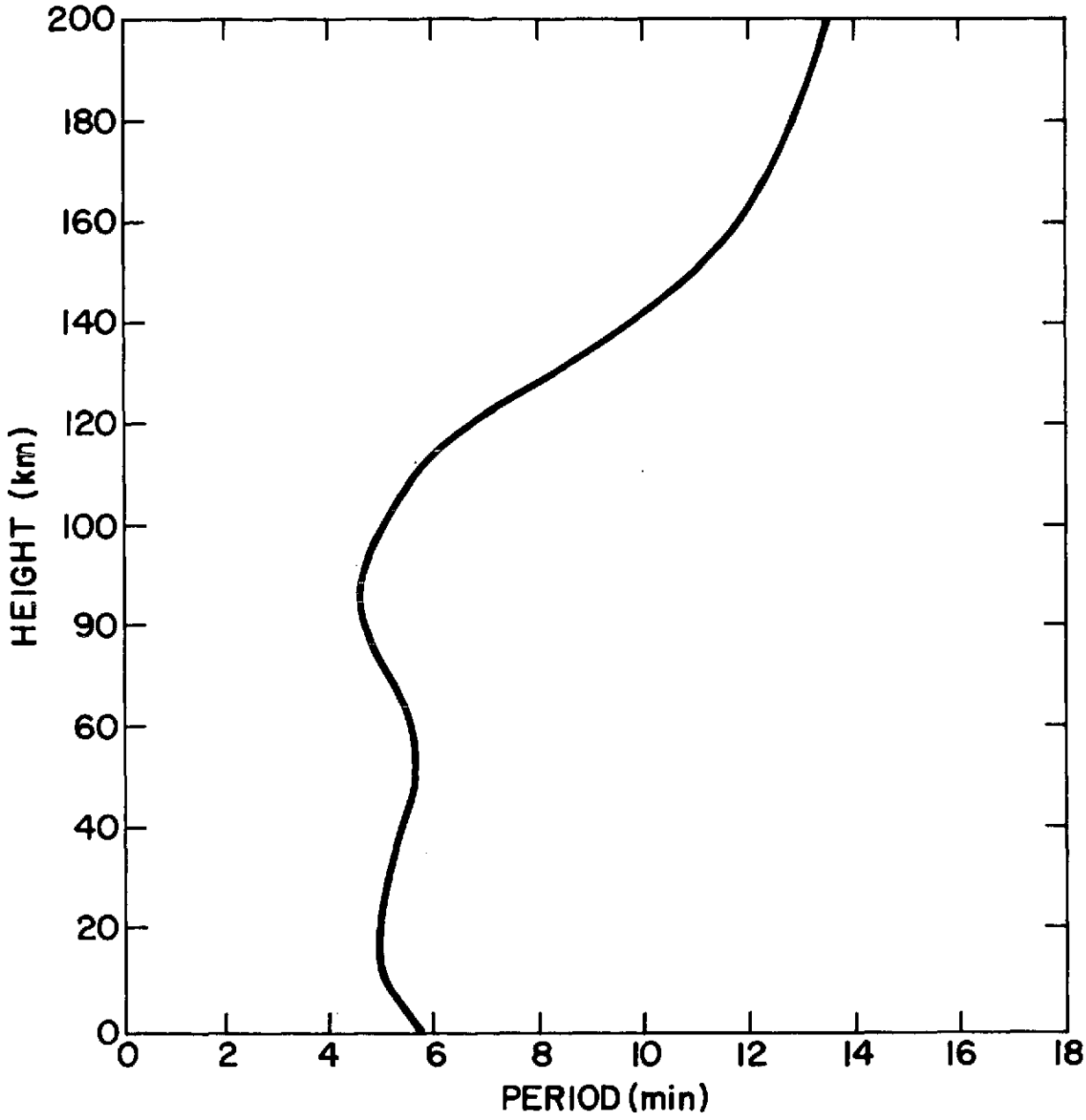

Figure 2.5. Period of the Brundt-Vaisala as a function of height, calculated using the 1962 U. S. Standard Atmosphere (adapted from *Georges* [1967]).

are not uniformly distributed, however, as is shown in Figure 2.6 [*Barnes*, 1972]. A meteor echo is most likely to occur at 98 km; 60% of all echoes occur at 95-99 km, and 90% at 90-100 km. Although these exact figures vary for different meteor-radar stations, the general shape of the distribution is maintained. Based on this distribution, the following conclusion is made: About 1000 echoes per hr are needed in order to resolve short-period waves near 95 km. Meteor-radar study of such short-period waves over the entire 80-120 km region requires a much higher echo return rate, on the order of 10,000 per hr. Lower frequency oscillations could be discriminated over a large height range without this high return rate, however.

2.3. *Measurement Accuracy*

The study of short-period gravity waves requires that the height, azimuth, and velocity of specular reflection points on meteor-trails be measured within certain tolerances, as discussed in Section 2.1. Since meteor-radar stations measure polar coordinates, the tolerance requirements for height and horizontal velocity measurements must be restated in terms of range, elevation angle, azimuth angle and radial velocity accuracies. In this section, each of the required system accuracies is considered in turn, and requirements for the polar coordinate measurement accuracies are developed.

2.3.1 *Height accuracy requirements.* Neglecting earth curvature, the height of a specular reflection point on a meteor trail is given by the relation

$$h = R \sin\zeta \tag{2.2}$$

where R is the radial range, and ζ the elevation angle (Figure 2.7). From

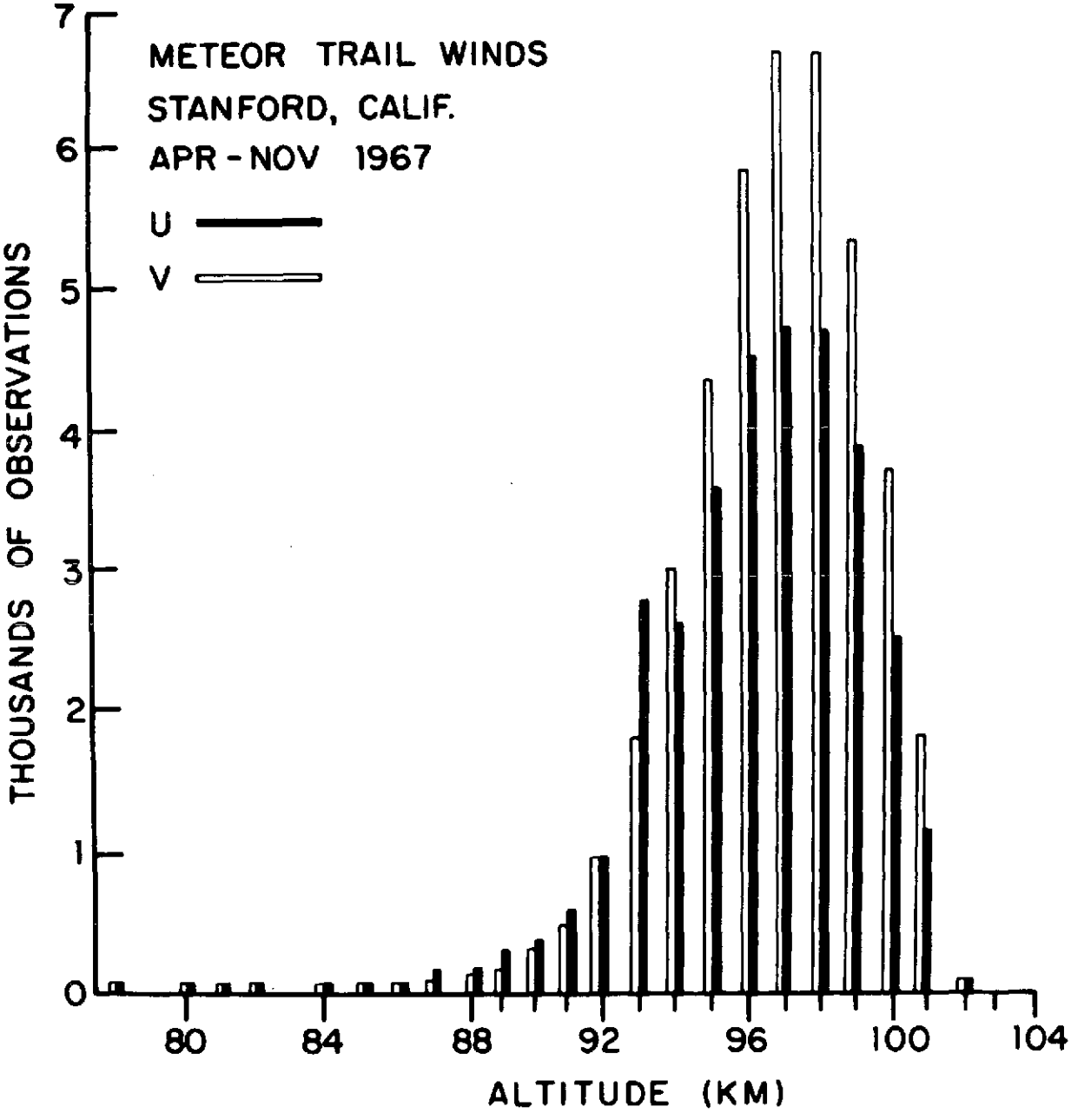

Figure 2.6. Meteor count versus altitude at Stanford [*Barnes*, 1972] where U is for east-west and V is for north-south winds.

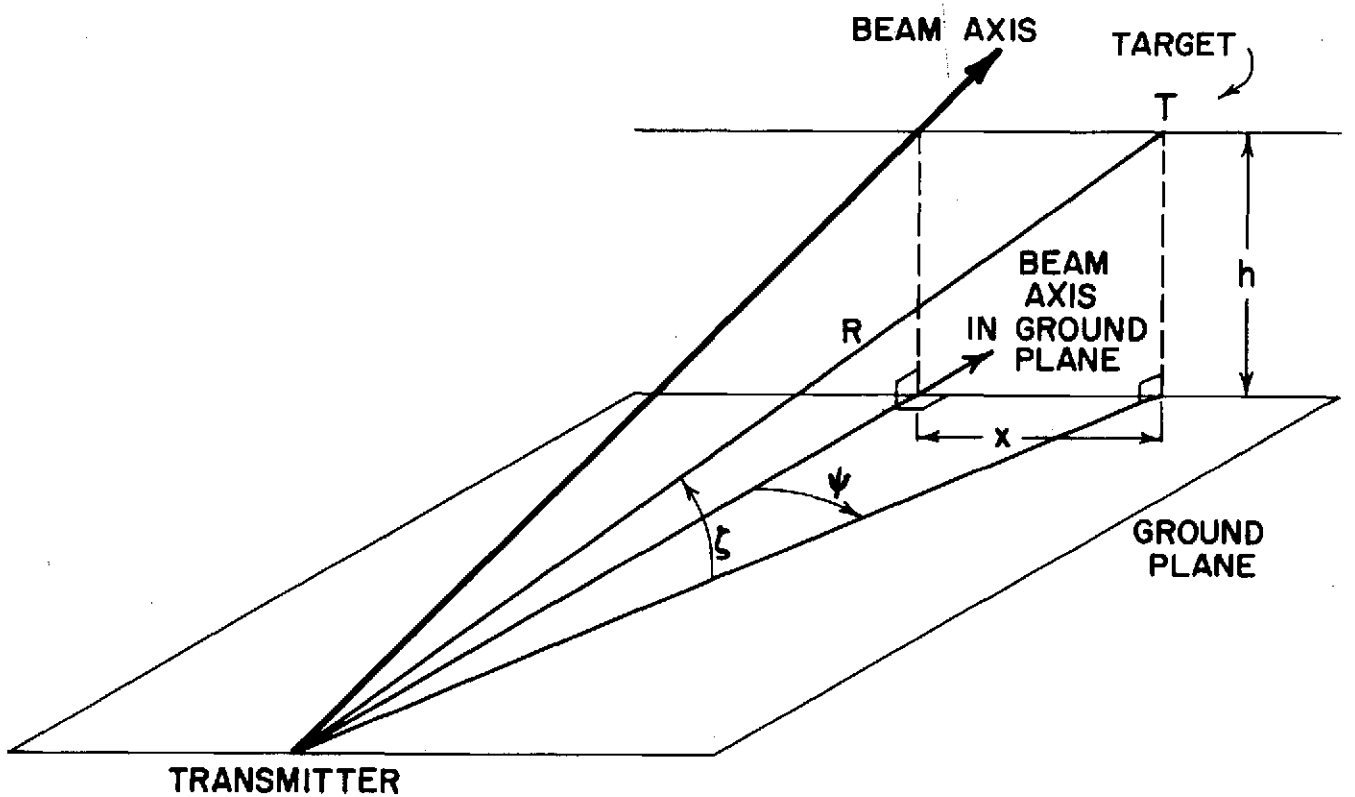

Figure 2.7. Illustration of the measurement coordinates.

Section 2.2, the most likely height of a meteor-trail reflection is about 98 km. The antennas for the Illinois meteor radar are aimed with their main lobes elevated at 45°. The representative radial range for meteor-trail echoes is therefore 98/sin 45°, or about 140 km.

The principal contribution to the total energy reflected from a straight-line meteor trail comes from the first Fresnel zone. This zone is the interval on the trail between the point of specular reflection, and the points where the range has increased by $\lambda/4$ over that to the specular point, where λ is the radar wavelength. The normal range differential of $\lambda/2$ for the end points of a Fresnel zone is halved in this case because of the round-trip path of the radar pulse. The width of this zone is $\sqrt{\lambda R/2}$ measured from the specular point along the trail. Because of symmetry, the zone from which the radar beam is reflected can be taken as a segment on the meteor trail of length $\sqrt{2\lambda R}$, centered on the specular point. For the Illinois meteor-wind system, the radar wavelength is 7.33 m. Using 140 km as the range, a representative dimension for the first Fresnel zone is calculated to be about 1.4 km; the vertical projection of this zone is about 1 km. The Doppler shift of a meteor-trail echo is therefore related to an average of the winds in the 1 km vertical projection interval. Because of this spatial averaging, a meteor radar is not capable of producing the vertical wind structure with as much detail as rocket releases.

A relation between height accuracy and range and elevation angle accuracies is found by differentiating equation 2.2:

$$dh = \frac{\partial h}{\partial R}\, dR + \frac{\partial h}{\partial \zeta}\, d\zeta$$

$$dh = \sin\zeta\, dR - R \cos\zeta\, d\zeta \qquad (2.3)$$

Then the error in height as a function of errors in range and elevation angle is given by

$$\Delta h \cong \sin\zeta\ \Delta R - R\cos\zeta\ \Delta\zeta \tag{2.4}$$

Assuming that ΔR and $\Delta\zeta$ are normally distributed about zero, the standard deviation of h is given by

$$\sigma_h = [(\sin\zeta\ \sigma_R)^2 + (R\cos\zeta\ \sigma_\zeta)^2]^{1/2} \tag{2.5}$$

where σ_h, σ_R, and σ_ζ are the standard deviations of the height, range and elevation angle measurements. The maximum acceptable value for σ_h was chosen as .5 km. This value is well under the Fresnel averaging interval, but large enough to be realistically achievable.

Taking R as 140 km and ζ as 45°, Table 2.2 gives some representative accuracies for range and elevation angle which produce the required height accuracy. The first and third table entries concentrate all of the error in the range and elevation angle error terms, respectively, of equation (2.2), while the second table entry corresponds to dividing the mean square error equally between each of the two error terms.

2.3.2. *Azimuth accuracy requirements.* In order to discriminate the spatial variation of short-period gravity waves, a horizontal resolution of 10-100 km is required [*Lindzen*, 1969]. This is obviously a very weak requirement relative to height accuracy; nevertheless a quantitative analysis is given below.

The horizontal displacement from due north, x, is given by

$$x = R\cos\zeta\ \sin\psi \tag{2.6}$$

Table 2.2

Accuracies for the elevation angle and range measurements which produce the required height accuracy.

σ_ζ (deg)	σ_R (km)	σ_h (km)
0	.7	.5
.2	.5	.5
.3	0	.5

where R is the radial range, ζ the elevation angle, and ψ the azimuth angle (Figure 2.7). Differentiating equation (2.6) gives the relation between horizontal displacement accuracy, and range, azimuth angle, and elevation angle accuracies. Because of the high accuracies required of the range and elevation angle measurements by the height tolerance, range and elevation angle accuracies should not contribute significantly to horizontal displacement error. Under this assumption, the following relation is derived from equation (2.6):

$$\sigma_x \cong |R \cos\zeta \cos\psi \, \sigma_\psi| \tag{2.7}$$

where σ_x and σ_ψ are the standard deviations of x and ψ. Using the same values for R and ζ as in Section 2.3.1,

$$\begin{aligned} \sigma_x &\cong 140^{*}.7 \cos\psi \, \sigma_\psi \\ &= 100 \cos\psi \, \sigma_\psi \\ &\leq 100 \, \sigma_\psi \\ \sigma_\psi &\geq .01 \, \sigma_x \end{aligned}$$

For a horizontal displacement accuracy of 10 km, σ_ψ must be about .1 radian, or about 6°. In comparison with the elevation angle measurement, azimuth angle tolerance is 20 times as great.

2.3.3 *Velocity accuracy requirements.* Table 2.1 gives some of the characteristics of winds in the meteor region. The mean wind velocity is less than about 60 $msec^{-1}$, and the maximum wave amplitude is about 50 $msec^{-1}$. The total horizontal wind should therefore be no larger than about 110-120 $msec^{-1}$. This assumption is supported by the experimental data shown in Figure 2.3. A meteor-wind system must, therefore, be capable of measuring

horizontal winds as high as 120 $msec^{-1}$. Meteor-radar systems, however, measure radial winds. If the vertical wind component is zero, the radial wind velocity is always less than the horizontal velocity. Assuming an elevation angle of 45°, radial winds are modified by a factor less than cos 45°, or about .7. The capability of measuring radial winds up to 100 $msec^{-1}$ in magnitude should therefore be sufficient.

Wind velocity accuracy must be a small fraction of atmospheric wave amplitudes, as mentioned in Section 2.1. Since wave amplitudes of about 50 $msec^{-1}$ will be studied horizontal velocity measurement accuracy of about 10 $msec^{-1}$ is required. Assuming an elevation angle of 45°, and an azimuth angle of 45° also, the radial wind is cos 45°·cos 45°, or only .5 of the total wind. Wind accuracy must therefore be .5·10, or 5 $msec^{-1}$, in order to measure winds with a horizontal accuracy better than 10 $msec^{-1}$ across the entire region of interest.

In summary, a meteor-radar system must be capable of measuring radial velocities up to about ±100 $msec^{-1}$ with an accuracy of 5 $msec^{-1}$.

2.4 *Processing System Requirements.*

The first constraint on the processing system is that it must keep up with the required rate of meteor returns. About 1000 echoes per hour are needed; therefore, the system must be able to collect and process the raw data from the radar system for at least 1000 returns per hour.

The output of the radar receiving system consists of actual meteor echoes and additive noise. The processing algorithms must operate on this noisy output signal, and produce the required measurement accuracies for azimuth angle, elevation angle, range, and velocity. Because of noise inherent in the receiving system, the signal-to-noise ratio of this output

signal can be no greater than about 40 dB. The processing algorithms are, therefore, constrained to require less than a 40 dB signal-to-noise ratio for the input signal in order to produce the measurement accuracies required.

3. SYSTEM DESCRIPTION

A large part of the hardware for the Illinois meteor-wind system is taken from the Havana meteor-wind system [*Hawkins*, 1963]. The Havana system was operated for 13 years as a joint project of the National Bureau of Standards, Harvard University, Smithsonian Astrophysical Observatory, and the National Aeronautics and Space Administration. When the Smithsonian program ended in 1971, the system hardware was transferred to the University of Illinois.

The arrangement of the Illinois meteor-wind system differs extensively from that of the Havana system. A major emphasis in the Illinois system is on moving as much of the control logic as possible out of the system hardware and into software, in order to achieve improved reliability. This is made possible by the availability of a medium-scale computer, capable of controlling the meteor radar; the computer has a good performance record as a programmed controller for a partial reflection system and a digital ionosonde.

This chapter describes the function of each software and hardware element in the system. In addition, the connection and interaction of all the elements is considered. The system hardware elements are first characterized; then the interconnection of these elements is given. The hardware-software interface and data-frame organization are described next. In the last section of this chapter, the software processing subsystems are described.

3.1 *Hardware Subsystems*

The system hardware is divided into three subsystems for ease of description: Transmitting, Receiving, and Processing. In the following sections, each is considered in turn.

3.1.1 *Transmitting.* The Illinois meteor-wind system uses a Continental Electronics model PO - 830 transmitter, operated at a fixed frequency of 40.92 MHz. This transmitter is pulse-modulated, and rated for a peak power output of 5 Mw. The nominal average power rating is 20 kw, and maximum average power 40 kw. The pulse width is constrained by the modulator to the range 3 to 100 μsec. In order to maintain the average power level at 20 kw, the corresponding pulse repetition frequency (PRF) is limited to the range 1330 to 40 Hz. The maximum signal bandwidth allowed by the transmitter license is 200 kHz. A pseudo-Gaussian pulse-shape is generated by the modulator in order to satisfy this requirement.

The transmitting antenna for the meteor-radar system is a twelve element dipole array, designed and constructed by Aeronomy Laboratory personnel. The elements are placed parallel in a single row, spaced by .537λ and elevated above the ground by .354λ. The main lobe of the antenna is oriented due north at an angle of 45° with the horizon. The antenna 3-dB beamwidth is 11.7° in elevation and 53° in azimuth at 100 km; the gain over a half-wave dipole is 18 dB. The antenna was designed to handle a peak power in excess of 5 Mw.

During both the design and and construction phases, provision was made for increasing the gain and horizontal directivity of the antenna by adding a second 12-element array beside the first. The antenna will be modified in this way if the initial data collected indicates such a change to be useful.

3.1.2 *Receiving.* In the Illinois System the angles of arrival of a radar echo from a meteor trail are measured by phase comparison of the received signals at spaced antennas [*Lee and Geller*, 1973]. The ground placement of the receiving antennas is shown in Figure 3.1. Antennas

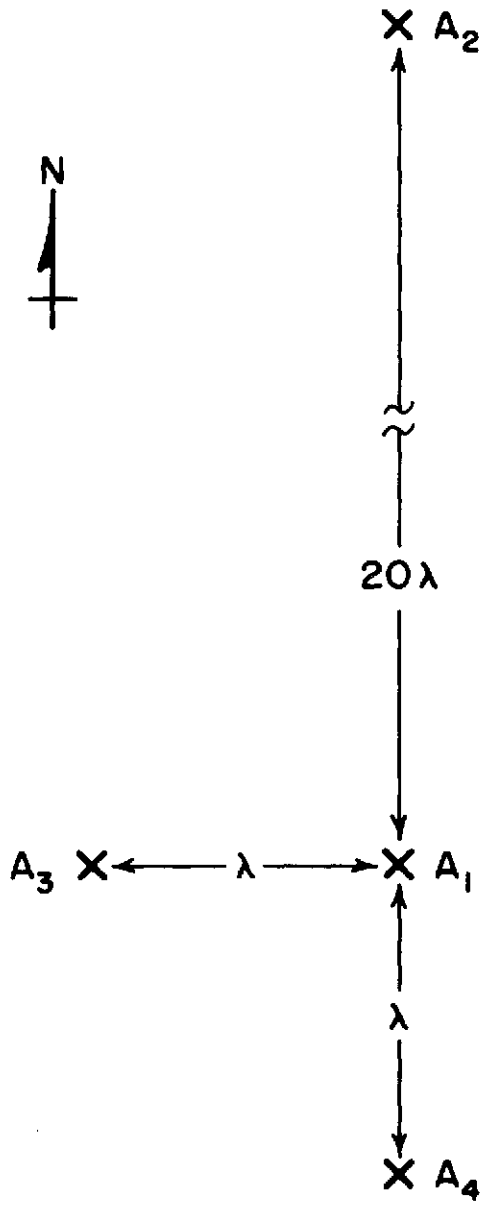

Figure 3.1. Receiving antenna ground placement.

A_1 and A_3 are spaced by one radar wavelength, and form the azimuth pair. Antennas A_1 and A_4 are also spaced by one wavelength, and form the elevation pair. In addition, antennas A_1 and A_2, spaced by 20 wavelengths, serve to refine the elevation angle measurement in order to satisfy the high elevation angle requirements. A 20-wavelength separation is used because of the requirement that elevation angle be measured with accuracy 20 times that of azimuth angle.

Four Telerex Model CY-13-40-42 Yagi antennas are used in the receiving system. These 13-element antennas have a gain of 15 dB. The 3-dB horizontal beamwidth is 30°, and the vertical beamwidth 64°. The antennas are mounted with phase centers at the points A_1 through A_4 on Figure 3.1. They are oriented due north, and elevated at 45°.

Four ARI PR 40-A receivers are used in the system. Each receiver has a fixed gain of 100 dB, a bandwidth of 180 kHz, and a noise figure less than 4 dB, and includes an envelope detector and two phase-comparator output channels. The envelope detector operates in two modes: linear and logarithmic. In the linear mode, it has a dynamic range of 30 dB, and the signal output at the top of the linear region is 1 V. The phase-comparator output channels produce signals proportional to the sine and cosine of the phase difference between the received signal and a reference input. The dynamic range and output of the phase-comparator channels are similar to those of the envelope detector.

Each receiver is connected to an antenna through a length of coaxial cable. The signal loss through the cable is 6 dB. For a sky-noise temperature of 10^4 K, the rms noise at the output of the receiver is .2 V. The receiver output noise with the input connected to a 50-Ω resistor

is .05 V. Then about 6 dB of attenuation is required at the input to each receiver, in addition to the 6 dB cable loss, in order to scale the input signal and make the maximum use of the receiver dynamic range.

3.1.3 *Processing.* The meteor-radar system is supported by a Digital Equipment Corporation Model PDP-15 digital computer system. The central processor of this system is an 18-bit machine, with 32 k words of .8-μsec core. An extended arithmetic element provides hardware multiply and divide. The machine has a real-time clock, and a data channel for high speed input/output.

Several basic peripherals are part of the system. Four DECtapes provide medium-speed bulk storage, and two disks are used for high-speed on-line storage. A 50-character-per-second paper-tape punch and a 300-character-per-second paper-tape reader are used for low-speed storage. Inputs are from a Teletype, Model KSR 35, which prints 10 characters per second, and a Hazeltine Model 2000 cathode ray terminal, which operates at 870 characters per second.

Analog input is provided by a Hewlett-Packard Model 5610 10-bit A/D converter. The device performs 10^5 conversions per second, and has a sampling aperture of .05 μsec. The A/D converter has an accuracy of $\pm 1/2$ least significant bit, and uses two's-complement output coding. A 16-channel input multiplexer selects a signal line to be sampled. Input signals in the range from -1 V to .998 V are mapped onto integers in the range from -512 to 511. The digital output of the converter enters the system through a direct-memory-access interface.

Digital input and output is also available. An interface allows 18-bit words to be sent or received by the processor through the accumulator.

The signals for the device are TTL logic levels. The maximum transfer rate for input or output is about 10^4 words/sec. Access to the input and output signals is provided by two connectors mounted on the front panel of the computer.

A Background/Foreground software monitor manages the system. The monitor supports assembly programming and FORTRAN IV compilation. All system peripherals are supported by the monitor, and all system programs are disk-resident for fast access.

An Automatic Priority Interrupt (API) system controls the asynchronous operation of the various peripheral devices and software tasks. Of the 8 priority levels available, the lowest four are assigned to software systems and the highest four to hardware devices. The software priority levels are used to set up a priority queue for processing real-time data, without inhibiting hardware interrupts from peripheral devices.

3.2 *Hardware Interconnection*

There are 12 receiver channels: two phase comparators and one envelope detector output for each of four receivers. However, there are only 9 unique information channels, since the signals in the four envelope-detector channels are essentially the same. The envelope-detector channel from the receiver connected to antenna 1 is used, and the other 3 are ignored. The information from the 8 phase-detector and one envelope-detector channels is sent to the A/D converter through the multiplexer.

In order to simplify the hardware system as much as possible, synchronous control is used. A master oscillator generates the pulse-repetition frequency, and the transmitter, multiplexer, and A/D converter are all synched to this oscillator (Figure 3.2). The operating sequence

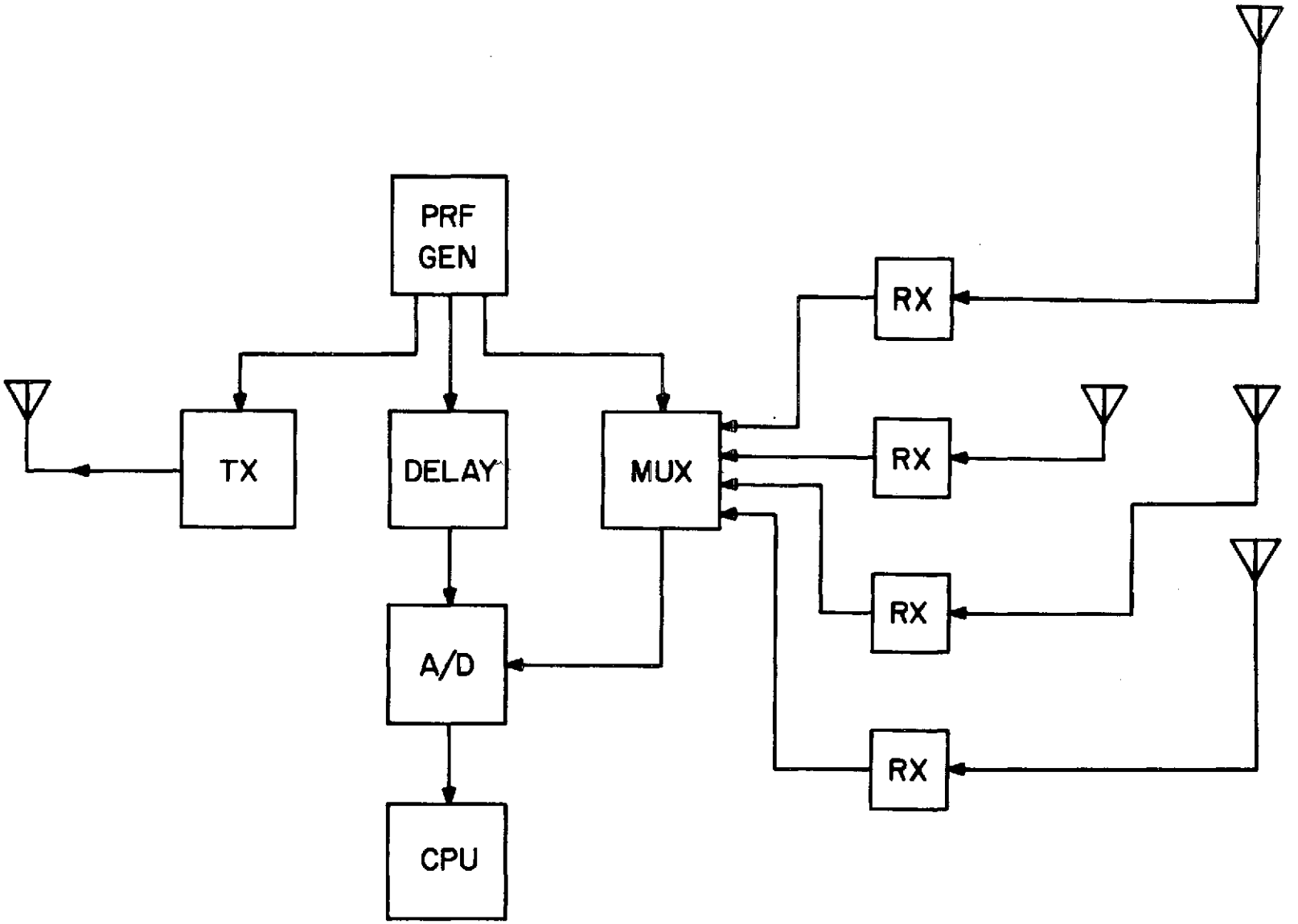

Figure 3.2. Hardware interconnection

is as follows: A pulse from the master oscillator causes an RF pulse to be transmitted, and also causes one channel to be selected by the multiplexer for input to the A/D converter. After a delay, the A/D converter begins sampling the selected channel, and sending the digital values corresponding to the input voltage at the sampling instant to the computer. The delay period is used to ignore echoes from objects too close to be meteor trails. After the required number of samples is taken corresponding to the radial region of interest, sampling ends. The sequence begins again with the next pulse generated by the master oscillator.

There are several consequences of this scheme. Note that the sequence is not affected by the data in the receiver channels. Whether or not an echo is present, the sequence continues. Secondly, for each pulse transmitted, only one channel is sampled. During the time when an echo is present, only 1/9 of the useful data is collected for each pulse transmitted. A third consequence is that an upper limit is placed on the useable PRF range. A pulse cannot be transmitted until sampling by the A/D converter is ended.

The delay period and sampling interval are selected by considering the region of interest (Figure 3.3). All meteor echoes come from the 80-120 km height interval. Considering the transmitting and receiving antenna elevation beamwidths, the range of elevation angles for received echoes is about $45° \pm 15°$. Then the minimum time after pulse transmission for which a meteor-trail echo can occur, T_{min}, is

$$T_{min} = \frac{2 \cdot 80}{\sin 60° \cdot c}$$

$$= 616 \text{ μsec}$$

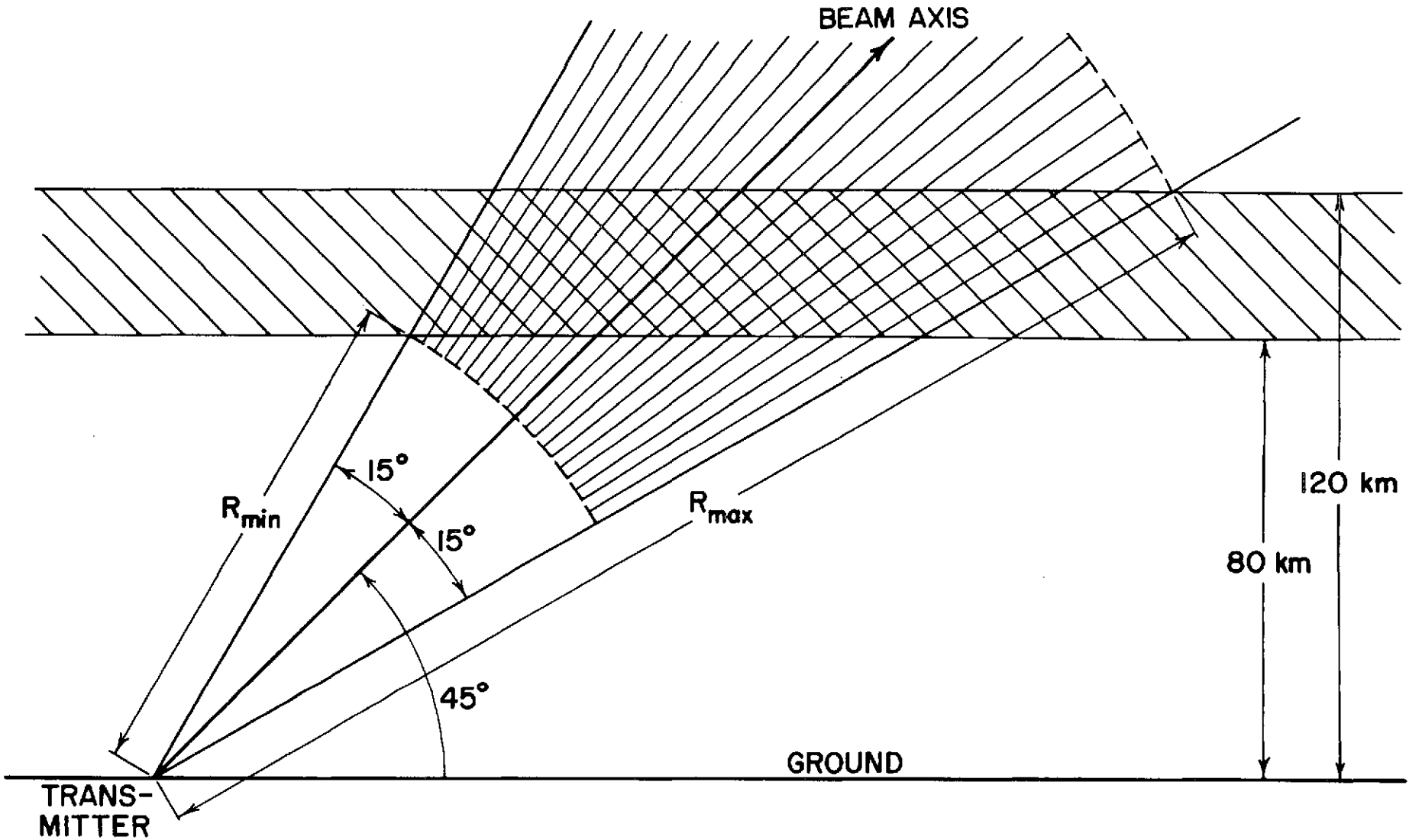

Figure 3.3. Meteor echo region.

where c is the speed of light. The factor of 2 in the numerator comes from the round-trip path of the radar pulse. The maximum time of interest after pulse transmission, T_{max}, is

$$T_{max} = \frac{2 \cdot 120}{\sin 30^\circ \cdot c}$$

$$= 1600 \text{ μsec} \quad .$$

The maximum usable PRF is simply T_{max}^{-1}, or 625 Hz. The A/D converter sampling period is the difference between T_{max} and T_{min}, or 984 μsec. This time period, however, must be a multiple of the A/D converter sampling interval, which is 10 μsec. Times T_{min} and T_{max} are, therefore, chosen as 610 and 1600 μsec, in order to cover the region of interest and still satisfy this requirement.

The various hardware elements must be interfaced. The reference signal into each of the receivers is simply the RF signal used by the transmitter. The receiver-output channels are connected directly to the multiplexer and the A/D converter, since the linear region for the receiver channels corresponds to the non-saturated region for the A/D converter (i.e., ±1 V). A TTL-level signal is needed to sequence multiplexer channels and also to initiate sampling by the A/D converter. The transmitter, however, requires a 5-V input pulse for triggering. The PRF generator delivers 5-V pulses. Therefore, an interface is needed between the PRF generator and the multiplexer. The delay element must accept a 5-V pulse as input, wait for 610 μsec, and then deliver a TTL-level signal to the A/D converter. This signal is the blanking pulse; it must have a "0" active state, and must remain in the "0" state for the

duration of the sampling period. A timing diagram of the required signals is given in Figure 3.4.

3.3 *Data Frame Organization*

In the data-collection system, a hierarchical data structure is used, consisting of elements, lines, and frames. A line is the sequence of digital values sent to the computer by the A/D converter during each sampling period. The individual values that form a line are elements. The sampling period covered by one line is T_{max}-T_{min}, 990 μsec. Elements are taken at 10-μsec intervals, starting at T_{min} and ending at T_{max}. A line is, therefore, a sequence of 100 elements. A frame consists of the number of lines required to measure all the parameters of one meteor-trail echo. Since there are 9 different receiver channels, at least 9 lines are needed to form one frame; in fact, more are required.

In order to determine the number of lines needed to make a frame, the requirements of the various measurement algorithms are considered. The echo-detection and range algorithm together require one line. Echoes are detected by searching a line taken from the receiver envelope-detector channel for elements with magnitude above a noise threshold; the range algorithm operates by considering the position in the line of these elements. The phase-comparison algorithm for antenna pairs requires four lines. These lines are taken sequentially from the sine and cosine channel of first one receiver, and then the other. In addition the Doppler frequency is needed. The Doppler frequency algorithm measures the change with time of the phase of the received signal at any of the four antennas. It requires that a total of four lines be collected alternately from the sine and cosine channels of any one receiver. Detailed descriptions of these algorithms are given in the next chapter.

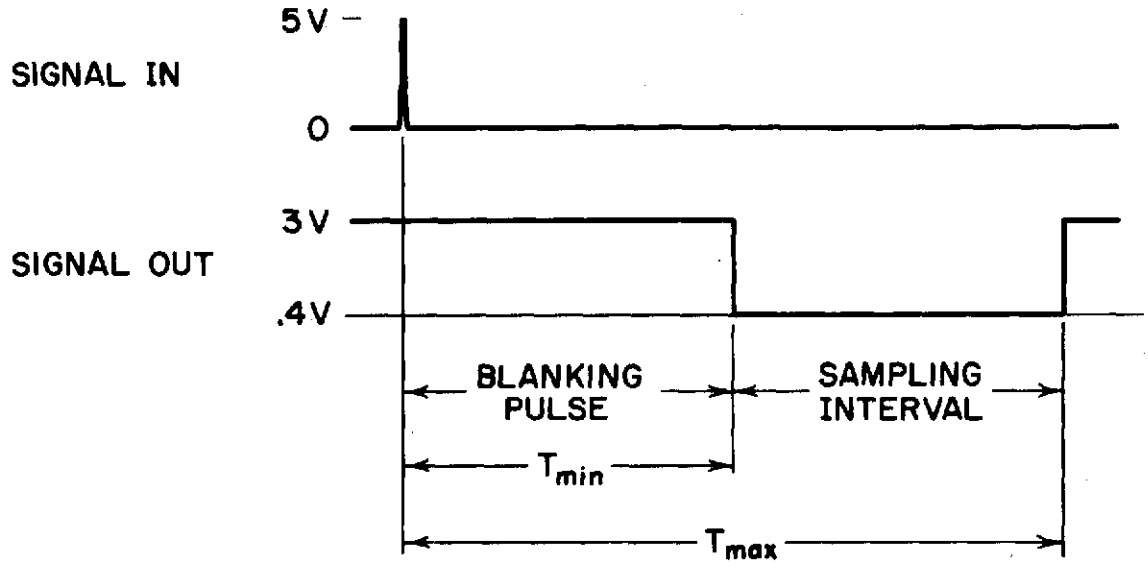

Figure 3.4. Delay element timing diagram.

Each frame must contain the data needed by a number of algorithms. Echo detection and range measurements must be made twice per frame to give good noise rejection. Three phase comparisons are needed: one each for the signals from the azimuth, coarse elevation, and fine elevation antenna pairs. The Doppler shift of each echo must be measured twice per frame, since the phase-comparison algorithm uses the Doppler measurement. The echo-detection algorithm uses one line, the Doppler and phase-comparison algorithms use four lines each. Then apparently 2 + 12 + 8, or 22 lines are needed per frame. By carefully arranging the order of the measurements in the frame so that some of the data lines are used by more than one algorithm, this number can be decreased.

The order of measurements is chosen with certain guidelines in mind. The two echo detection and range measurements should be well separated in the frame so that any noise present in the first line will be decorrelated from that in the second. Also, the fine-elevation phase comparison should be preceded and followed by a Doppler measurement, since this phase comparison is the most critical, and the phase-comparison algorithm accuracy is strongly related to Doppler accuracy.

Using S_i and C_i to symbolize lines taken from the sine and cosine channels respectively of the receiver connected to antenna i, and V as the video output of the envelope-detector channel, Figure 3.5 shows a sequence of 16 lines which hold the data for the required measurements in the proper sequence. The total data frame is, therefore, 16 lines of 100 elements, for a total of 1600 elements; one data frame is collected for every 16 pulses transmitted. Since exactly 16 lines are needed, the 16-channel multiplexer can be used to good advantage. Each receiver

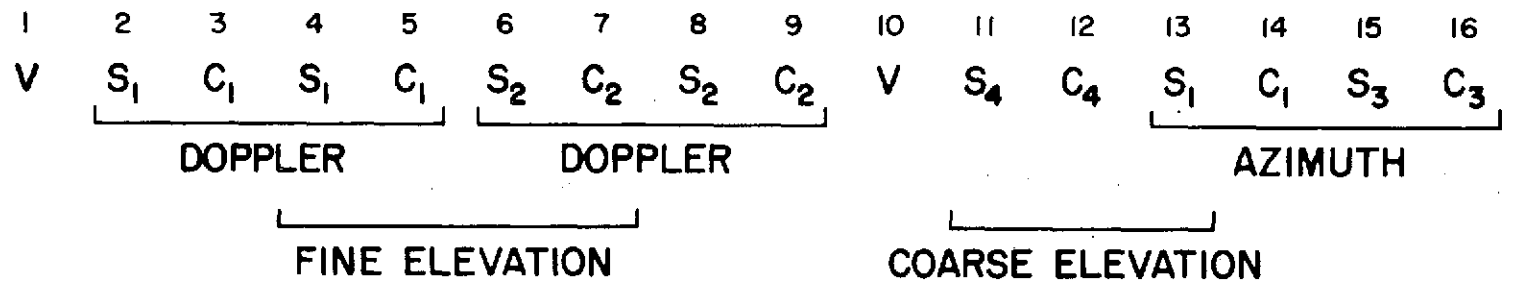

Figure 3.5. Receiver channel multiplexing sequence.

channel is connected to the multiplexer channel corresponding to its position in the 16-line sequence shown in Figure 3.5. Note that some of the receiver channels are connected to more than one multiplexer channel. With the receiver channels connected to the multiplexer in this way, the multiplexer simply sequences through each of its input channels in order. One pass through all the input channels produces one data frame.

3.4 *Data Processing Subsystems*

The data processing system (Figure 3.6) is made up of three parts: collection, search, and reduction. The collection program controls the A/D converter and runs at the highest priority level. This program operates synchronously with the hardware system. Lines are collected from the A/D converter until a full frame is available; then, control is passed to the echo-search program at a lower priority level. Collection continues even while the echo-search program is running, since the priority level of the collection program allows all other programs to be interrupted whenever necessary. The echo-search program scans the two video-output lines of the frame. If an element above the noise threshold is found, a reduced frame is built; otherwise the frame is discarded. A reduced frame is made up of certain essential elements taken from the total frame, which characterize the echo. Each reduced frame is pushed onto a first-in, first-out stack for temporary storage. The reduction program takes a reduced frame as input data, and produces the polar coordinates and velocity of meteor-trail echoes.

There are three main data storage areas. The first is the frame storage buffer. Data are written into this region by the collection

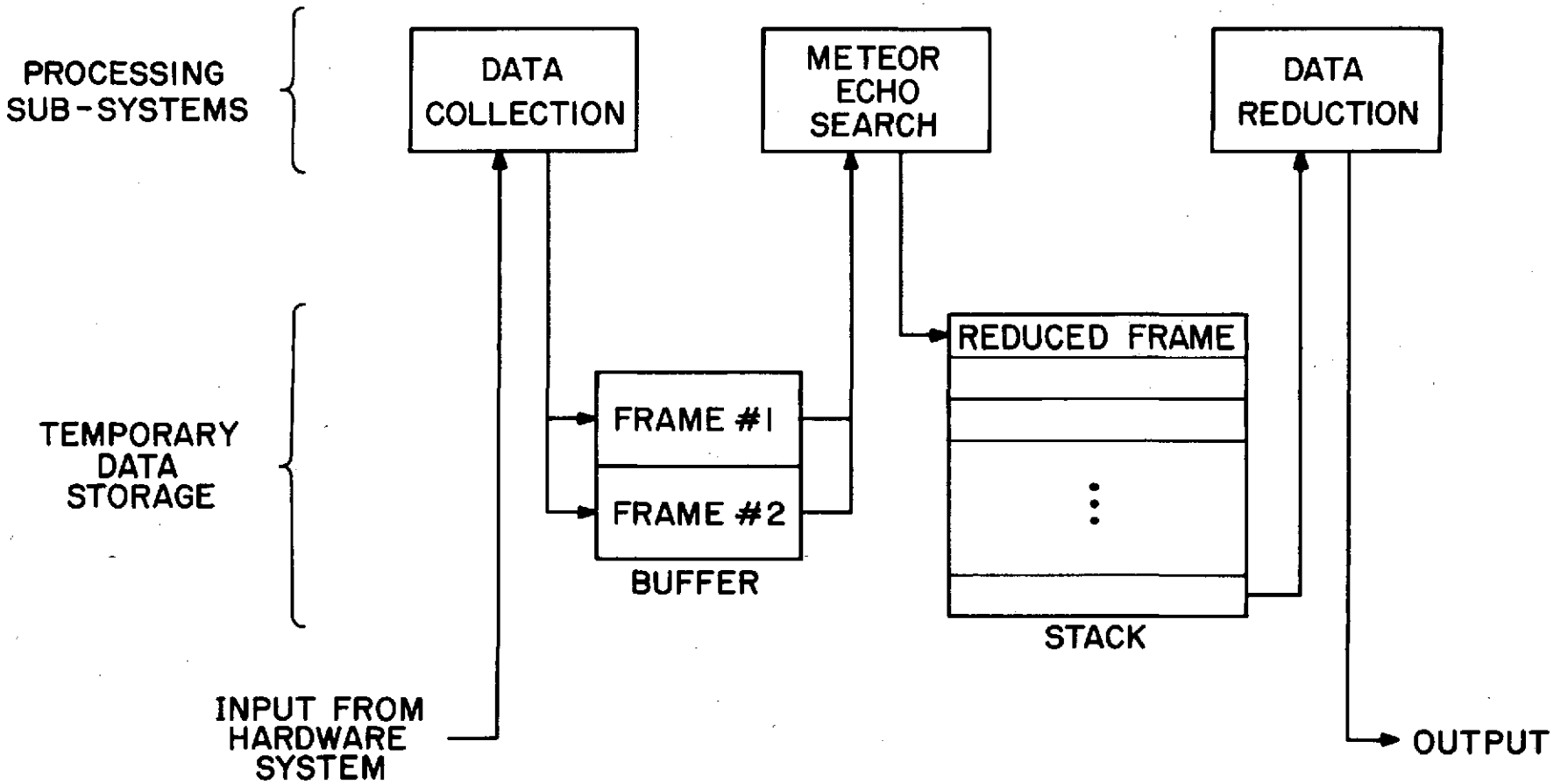

Figure 3.6. Data processing system interconnection.

program, and read by the range search and echo detection subsystem. Since concurrent collection and echo search is needed, a double buffer is used. That is, collection and search are done alternately in two buffers. Since one frame has 1600 elements, a 3200 word storage area is needed. The second major storage area is the first-in, first-out stack. The echo detection and range program produces a 22-element reduced frame, which is stored temporarily in this stack, until the data reduction program is ready to accept this information as input data. The stack has 220 words, enough memory to store 10 reduced frames. The third major storage area is the system status table. This table is only 10 words long, but it contains all the information needed for communications between the various subsystems. The function of each word is given in Table 3.1.

These three storage blocks are Fortran Named Common storage areas; the frame buffer is called FRAME, the stack is named STACK, and the status table is named STATUS. Only STATUS is initialized by a BLOCK DATA subprogram.

Program modularity is an important consideration in real-time data processing systems, since changes are often made. By breaking the system into small modules, each performing one particular function, modifications are easily made, and unexpected side effects from small changes are avoided. With this in mind, two rules are imposed on the software coding:

1) No single program or subprogram shall have more than 50 executable lines.

Table 3.1

Word definitions for the system status table

Word	Function
1	Time in seconds since start of collection
2	Pointer to current line being filled
3	Pointer to current frame being frame being filled
4	Pointer to last reduced frame written on stack
5	Pointer to last reduced frame read from stack
6	not yet assigned
7	
8	
9	
10	

2) No program or subprogram shall have more than one entry point.

3.4.1 *Data collection.* The data collection program is an interrupt service routine for the A/D converter. Each time a line is completed, the processor is interrupted and the collection program is executed. After the collection program is finished, the interrupted program is restarted. The collection program performs two operations. First, the A/D converter is set up to collect the next line. Then, if a frame has just been completed, the echo search and range program is started. Figure 3.7 is a flow chart of the collection program. In this figure, J is a pointer to the current line.

3.4.2 *Meteor echo search.* The maximum-amplitude element in a video line, along with the elements immediately preceding and following, is called the range set. If the location in a video line of the maximum amplitude element is position i, then the range set for this line is the group of elements i-1, i, and i+1. The meteor echo search begins with selection of the range set in the first video line. Next, elements i-1, i, and i+1 are selected from the second video line. A threshold test is done next. If the element in position i of both video lines is above the noise threshold, and neither is saturated (that is, neither has a value of 511 or -512) then a usable meteor trail echo is present. If no such echo is present, the frame is discarded. If a trail echo is present, however, the following actions are taken. The six elements taken from the two video lines are pushed onto the stack, along with i, the position of the center sample in the first video channel range set.

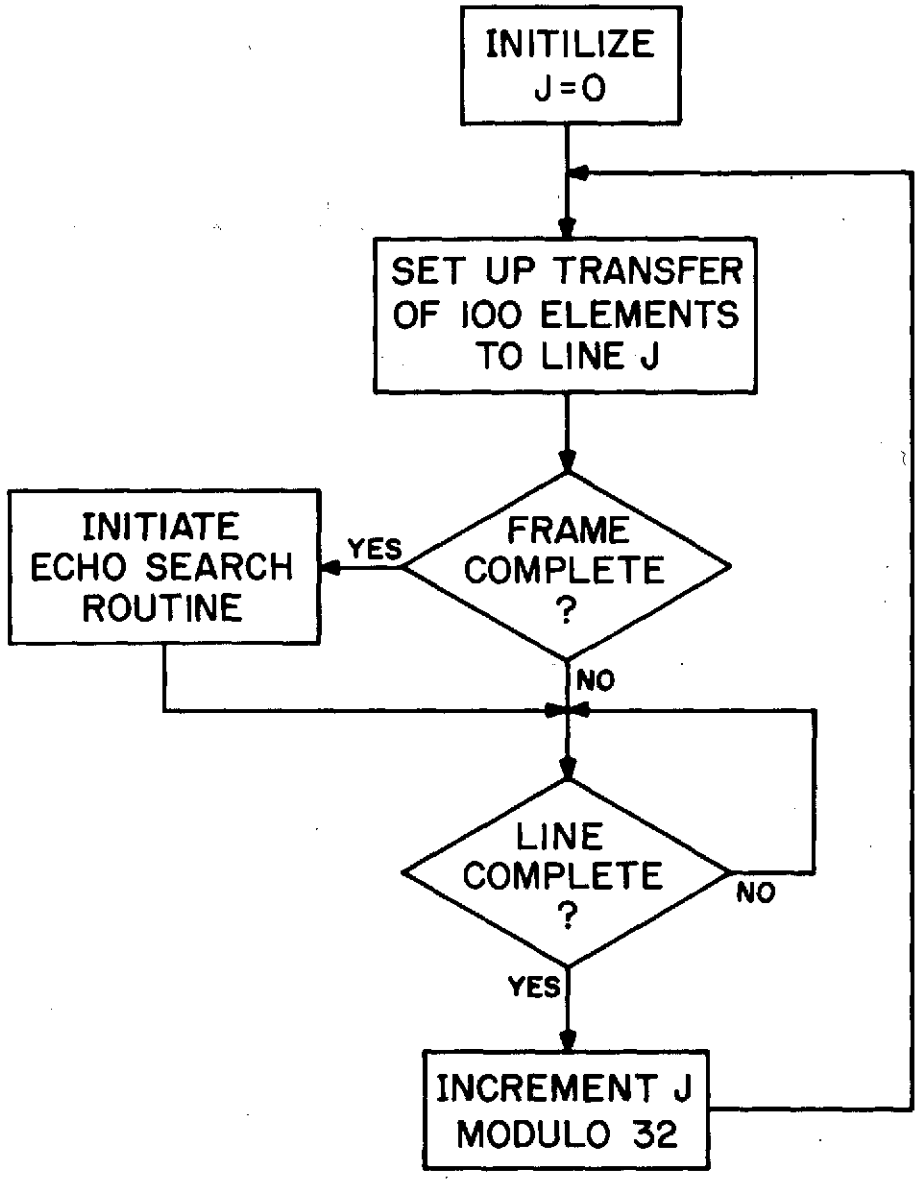

Figure 3.7. Data collection routine.

Each of the elements in position i of the 14 sine and cosine lines are also added to the stack. Finally, the current time in seconds relative to the beginning of data collection is put on the stack. Altogether, 22 samples are recorded. These 22 samples form one reduced frame. A flow chart of this algorithm is shown in Figure 3.8.

3.4.3 *Data reduction.* The data-reduction subsystem takes reduced frames from the stack, and calculates the polar coordinates and radial velocity of meteor-trail echoes. The program uses all the data reduction algorithms which are described in the next chapter; each algorithm is a subroutine.

The reduction program itself does four things: it interfaces to the stack, formats the data for the algorithm subroutines, performs consistency checks on the redundant frame measurements, and writes the results of the reduction onto magnetic tape.

The range algorithm is applied to the data from both video lines. A consistency check is made on the results; if the results do not agree within the required range accuracy of 700 m, the reduced frame is rejected and no further processing is done. If the consistency test is passed, the Doppler algorithm is applied to both Doppler data sets. Again, a consistency check is made; the results must agree to within 5 $msec^{-1}$. The various phase comparisons for the antenna pairs are then made, after which the phase differences for the antenna pairs are combined with antenna spacing information to give the angles of arrival. Finally, all of the results are written onto magnetic tape. A flow chart of the reduction subsystem is shown in Figure 3.9.

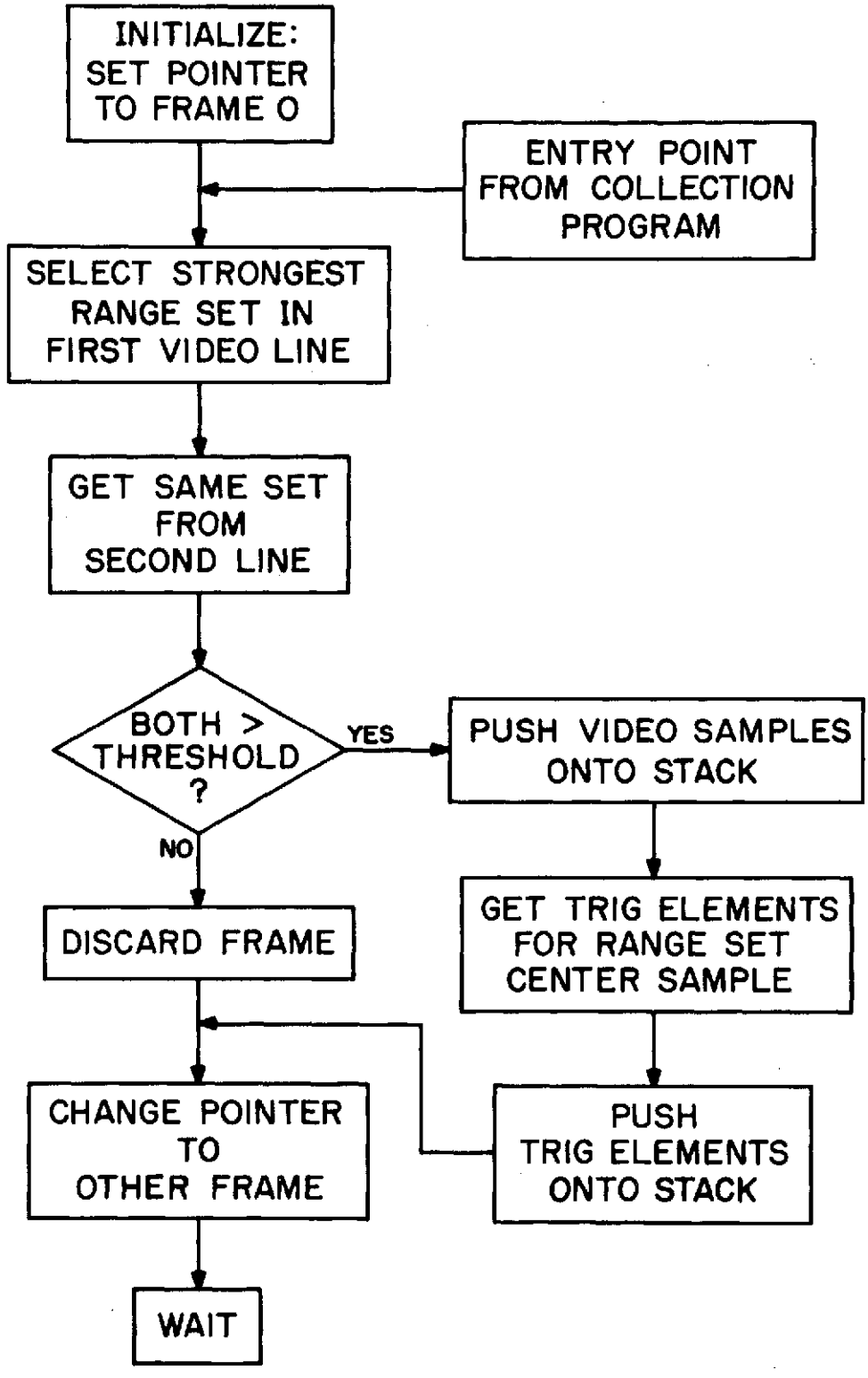

Figure 3.8. Meteor echo search routine.

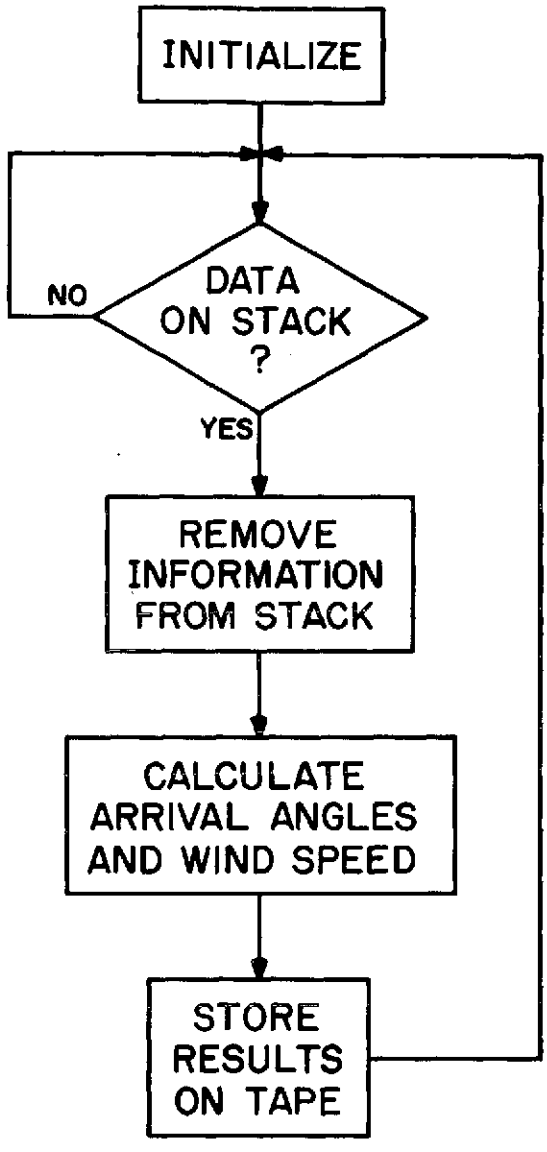

Figure 3.9. Data reduction routine.

4. MEASUREMENT ALGORITHMS

This chapter describes in detail each of the four measurement algorithms which are used in the processing system. The measurement accuracy and magnitude limitations of the algorithms are also considered. The effect of the PRF and pulse width on measurement accuracy is examined, and the pulse width and PRF which optimize measurement accuracy are found.

4.1 *Range Determination by Curve Fitting*

In meteor radar, range is deduced from the time difference between the instant of pulse transmission and the instant of echo reception. The instant of pulse transmission is that instant during pulse transmission when the maximum voltage is present at the transmitting antenna terminals, while the instant of echo reception is that instant during echo reception when the maximum voltage is present at the envelope detector video output. Range is calculated by multiplying this time difference by $c/2$. Of course, any system delays introduced by the receiver or interconnecting cables must be subtracted from the time difference before the range calculation.

In the Illinois system, the time difference is measured in three parts. First, there is the 610-μsec duration of the blanking pulse (Section 3.2) established to reject radar clutter. Second, there is the time between collection of the first element in the video line, at the end of the blanking pulse, and the instant of sampling of the largest element in the line. The elements are samples taken at equal 10-μsec intervals, so if the Nth element is the largest, this second time interval is $10(N-1)$μsec. The instant the largest sample is taken does

not correspond exactly with the instant the largest voltage is present at the receiver video output; so a third part of the time difference, τ (Figure 4.1) corresponds to the interval between the largest voltage, and the instant the largest element is sampled. Range is calculated according to the expression

$$R = (610 + 10(N - 1) + \tau) \cdot 1.5 \qquad (4.1)$$

where R is the range in kilometers, and τ is in μsec. For a symmetric pulse, τ is in the range ±5 μsec. If τ is assumed zero, the range may be in error by ±750 m. Recall from Section 2.3.1 that the required range accuracy is ±500 m. Therefore, some method is needed for measuring τ. This method is the range algorithm, which uses a process of curve fitting. Two aspects of the sampling of the video output must be considered before fitting a curve to the sampled elements. These aspects are the finite aperture time and sampling rate of the A/D converter, and are discussed in the following paragraphs.

The finite aperture time of the A/D converter causes an integration of the input signal; however, the video-output voltage is slowly varying relative to the .05-μsec aperture time of the A/D converter since the receiver has a 180-kHz bandwidth. Then the output of the A/D converter is a good approximation to the input voltage at the instant of sampling, and the finite aperture time has little effect on sample accuracy.

The radar system has a characteristic pulse shape, defined as the time record of the voltage at the receiver video output during reception of an echo from a hard reflector. This shape is determined only by the

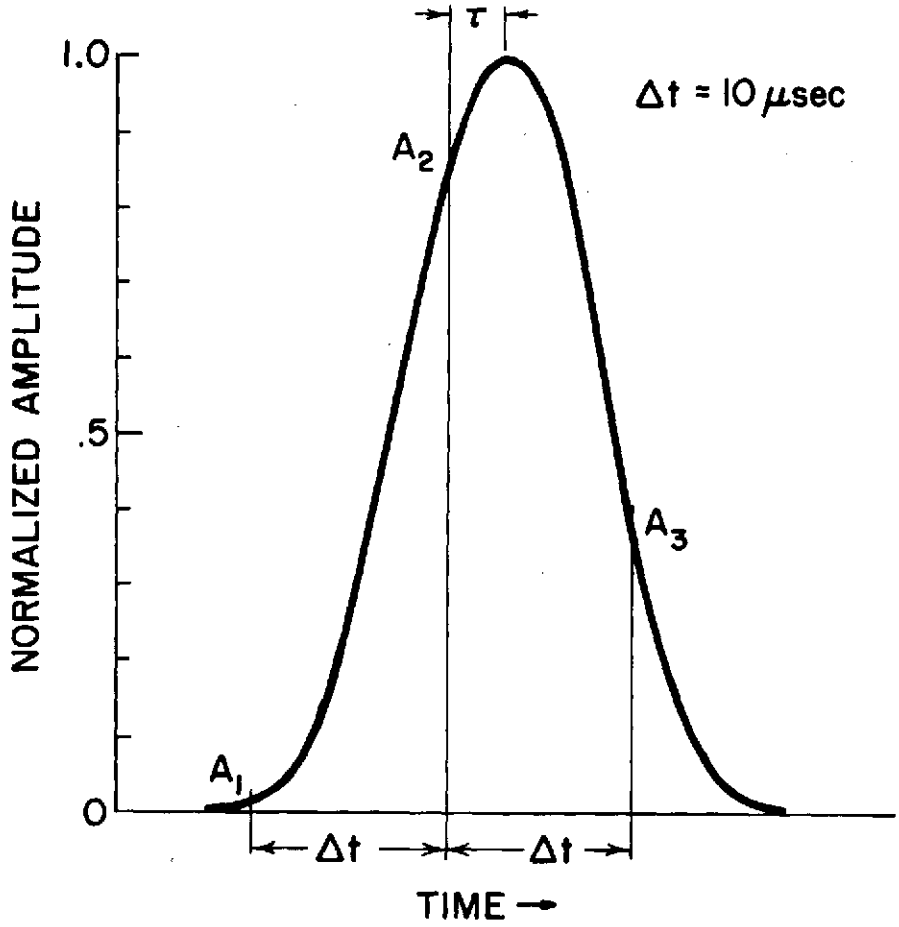

Figure 4.1. Typical receiver output pulse, with sampling superimposed. The quantity τ is the offset between point of maximum on the pulse, and highest sample, and A_1, A_2, and A_3 are the values of samples occurring during pulse reception.

transmitted pulse shape and the receiver bandpass, and is the convolution of the receiver impulse response with the transmitted pulse. Of course, convolution in the time domain is simply multiplication in the frequency domain. Both the receiver bandpass and the transmitted pulse are nearly Gaussian. Using the following Fourier-transform pair, the characteristic pulse can be calculated from the receiver bandpass and the transmitted pulse:

$$g(t) = \left(\frac{s}{\pi}\right)^{1/2} \exp(-st^2) \leftrightarrow G(f) = \exp\left[\frac{-\pi^2 f^2}{s}\right] \tag{4.2}$$

The transmitted pulse is transformed to the frequency domain and then multiplied with the receiver bandpass. The product is then transformed to the time domain, giving the characteristic pulse. For a Gaussian receiver bandpass and transmitted pulse, the characteristic pulse is also Gaussian. By comparing the characteristic pulse with the transmitted pulse, the shape modification due to the receiver is found. The ratio r_L of the characteristic pulse length to the transmitted pulse length, and the ratio r_A of the characteristic pulse maximum amplitude to the transmitted pulse maximum amplitude, are given by

$$r_L = [1 + (\pi BL)^{-2}]^{1/2} \tag{4.3}$$

$$r_A = [1 + (\pi BL)^{-2}]^{-1/2} \tag{4.4}$$

where B is the receiver bandwidth and L the transmitted pulse width. The level used to define the bandwidth and pulse width is arbitrary; however, the same level must be used in both definitions. Also, consistent units are required, i.e.: Hz and sec, MHz and μsec.

The sampling rate of the A/D converter is 10^5 sec^{-1}, so if the characteristic pulse is less than 10-μsec wide, sampling may miss the pulse entirely. For a pulse width of 10-20 μsec, at least one sample will always occur during pulse reception; for a width of 20-30 μsec, at least two will occur; for a pulse width greater than 30 μsec, three or more samples will occur during pulse reception. There is no way to compute τ if the pulse width is under 20 μsec.

A technique for finding τ is available if three criteria are met: 1) The characteristic pulse shape is known. 2) The characteristic pulse width is such that more than one sample is taken in its duration. 3) The received echo is from a hard reflector. Under these conditions, the time record of the video output can be reconstructed from the samples taken during pulse reception. This reconstruction amounts to fitting the known characteristic pulse to the samples. Once the time record of the video output has been reconstructed, the quantity τ is readily available. Since samples need only be above the noise level to be used in the pulse fitting, the width of the characteristic pulse is defined as the time between 20-dB points. The pulse fitting method used for pulse widths in the range from 20-30 μsec takes the ratio of the maximum element to the higher of its two neighbors. The method used for pulse widths greater than 30 μsec fits a parabola to the maximum element and its two immediate neighbors. The meteor-wind system uses the parabola method, for reasons given in Section 6.1. Both methods are described below, however, for completeness.

4.1.1 *Parabola method.* The parabola method assumes that the shape of the characteristic pulse between 20-dB points can be modeled successfully by a parabola. For the Gaussian-shaped pulse that the meteor-radar transmitter produces, this assumption is reasonable. The procedure for finding τ is to first find the coefficients of the function $f(x) = ax^2 + bx + c$, which passes through the maximum element, and each of its immediate neighbors. The first derivative $f'(x)$ is found; τ is equal to the value of x for which $f'(x) = 0$. Elements A_1, A_2, and A_3 are the three points to which the parabola is fitted (Figure 4.1). Relative to the center element, A_1 and A_3 are taken at $x = -10$ and $x = 10$, respectively. Then three equations can be written.

$$\begin{aligned} a(-10)^2 + b(-10) + c &= A_1 \\ a(0)^2 + b(0) + c &= A_2 \\ a(10)^2 + b(10) + c &= A_3 \end{aligned}$$

These equations are then simplified and solved.

$$\begin{aligned} \begin{bmatrix} 100 & -10 \\ 100 & 10 \end{bmatrix} \begin{bmatrix} a \\ b \end{bmatrix} &= \begin{bmatrix} A_1 - A_2 \\ A_3 - A_2 \end{bmatrix} \\ \frac{1}{100} \begin{bmatrix} 1/2 & 1/2 \\ -5 & 5 \end{bmatrix} \begin{bmatrix} A_1 - A_2 \\ A_3 - A_2 \end{bmatrix} &= \begin{bmatrix} a \\ b \end{bmatrix} \end{aligned} \tag{4.5}$$

The first derivative is calculated and set to zero:

$$f'(x) = 2ax + b$$

$$f'(\tau) = 0$$

$$\tau = \frac{-b}{2a} \tag{4.6}$$

Quantities a and b are substituted from equation (4.5):

$$\tau = 5 \cdot \frac{A_1 - A_3}{A_1 + A_3 - 2A_2} \tag{4.7}$$

Then the offset τ, in μsec, is found according to equation (4.7). Note that the parabola method does not require prior knowledge of the characteristic pulse shape. Even if the pulse shape is distorted by reflector irregularities, the method still gives a reasonable approximation to τ. The only limitation is the modeling of the pulse shape between 20-dB points by a parabola. For a Gaussian-shape characteristic pulse, 30 μsec wide, the maximum error in τ due to parabola modeling is 1 μsec. For no-noise conditions, then, the parabola-fitting technique gives a range accuracy of ±150 m; this accuracy degrades gracefully with pulse distortion and atmospheric noise.

4.1.2 *Ratio method.* If the characteristic pulse is 20-30 μsec wide, only two samples will be taken during pulse reception; finding τ by a parabola fit is not possible. If the shape of the pulse is known, however, the ratio of the two samples can be used to imply τ. For any given pulse shape, a table can be formed which relates τ to the ratio of the two samples. For a symmetric pulse, the points of pulse maximum must occur somewhere in the closed interval between the maximum sample, and the midpoint between the two samples; that is, $0 \leq |\tau| \leq 5$ μsec.

Table 4.1 is developed by assuming that a Gaussian pulse is transmitted, and that the receiver has a Gaussian bandpass. For various receiver bandwidths, the ratio for several values of τ is given. Negative values of τ are not given, because in this case the table entry is just the reciprocal of that for positive τ.

The accuracy limitations of this technique are twofold. First, the largest practical size for the table is about 6 elements as shown, implying an accuracy of 1 μsec in τ. Second, pulse distortion and noise introduce large errors. For these reasons, the ratio technique is limited to an accuracy of about ±2 μsec. The corresponding range accuracy is ±300 m.

4.1.3 *Conclusion.* For the range algorithm, the parabola and ratio methods both give satisfactory results. The parabola method, however, is less susceptible to errors from pulse distortion and low signal-to-noise ratio then the ratio method and seems to be the optimal technique. For a given transmitter average power, a wide pulse implies a low PRF. It is shown in the following subsections, however, that the Doppler and phase-comparison algorithms are most accurate when a high PRF is used. The selection of the optimal pulse width and PRF must be deferred until the accuracy of the entire system has been considered. The final selection is made in Section 6.

4.2 *Doppler Measurement*

Each system receiver has a phase comparator. Phase comparisons are made between receiver IF signals and a 5.5 MHz signal derived from and phase-synchronous with the transmitter oscillator. The frequency of the IF signal in each receiver is 5.5 MHz plus the Doppler shift of the

Table 4.1

Ratio of the highest sample to the higher of its two neighbors for offset τ in the range 0-5 μsec, and receiver bandwidth in the range 20-150 kHz. Transmitted pulse width is 5 μsec. Transmitted pulse and receiver bandpass are Gaussian.

		Offset (microseconds)					
		0	1	2	3	4	5
Bandwidth (kHz)	20	1.43	1.33	1.24	1.16	1.08	1.00
	50	4.60	3.39	2.50	1.84	1.36	1.00
	75	10.23	6.42	4.04	2.53	1.59	1.00
	100	17.22	9.75	5.52	3.12	1.77	1.00
	150	29.65	15.05	7.64	3.88	1.97	1.00

received signal. The phase comparators produce two outputs, signals proportional to the sine and cosine of the phase difference between the IF signals and the reference input. The time derivative of the phase at any of the receivers is the Doppler-frequency shift of the received signal. A method for calculating this time derivative from elements taken from the sine and cosine outputs of one of the phase comparators during echo reception is needed. This method is the Doppler algorithm.

The outputs of any phase comparator at some instant t can be written

$$A \cos(\theta + \omega t)$$

$$A \sin(\theta + \omega t)$$

where A = amplitude

ω = Doppler frequency

θ = phase of signal at antenna

Doppler frequency is measured as follows: at time t_1, measure the cosine-output signal; at time t_2, measure the sine-output signal; at time t_3, measure the cosine-output signal again. These measurements are labeled M_1, M_2, M_3; the Doppler frequency is given by the relation (Appendix I)

$$\omega = \frac{\sin^{-1} Z'}{\Delta t} \tag{4.8}$$

where $$Z' = \frac{M_1 - M_3}{2 M_2}$$

$\Delta t = t_2 - t_1 = t_3 - t_2$ = pulse repetition period

$$M_1 = A \sin(\theta + \omega t_1)$$

$$M_2 = A \cos(\theta + \omega t_2)$$

$$M_3 = A \sin(\theta + \omega t_3)$$

Quantities M_1, M_2, and M_3 are input through the A/D converter, causing some quantization error in each. The worst-case error in Z' due to quantization of M_1, M_2, and M_3 is calculated in Appendix II, with the result

$$|\Delta Z'| \leq \left| \frac{1/2 + \sin|\omega\Delta t|}{M_2} \right| \tag{4.9}$$

At this point, it is covenient to define a quantity α, the Doppler angle, as the phase change due to Doppler shift at any receiver in each pulse-repetition period. That is,

$$\alpha = \omega\Delta t$$

Then the expression for $\Delta Z'$ is rewritten

$$|\Delta Z'| = \left| \frac{1/2 + \sin|\alpha|}{M_2} \right| \tag{4.10}$$

Note that the denominator in this expression can be small; large errors in Z' result. If a fourth measurement, $M_4 = \cos(\theta + \omega t_4)$, is taken, an alternative method of finding $\sin \omega\Delta t$ is available. A trigonometric argument similar to that in Appendix I gives

$$Z'' = \frac{M_4 - M_2}{2M_3} = \sin \omega\Delta t \tag{4.11}$$

Quantization error in this expression is given by

$$|\Delta Z''| \leq \left| \frac{1/2 + \sin|\alpha|}{M_3} \right| \tag{4.12}$$

Both $\Delta Z'$ and $\Delta Z''$ are of the same form, and differ only in the denominator. The method for finding sin $\omega\Delta t$ which gives the least error is, therefore, the method which has the largest denominator. Two new quantities, Z and M, are defined:

$$\text{if } |M_2| > |M_3| \quad , \quad M = M_2 \quad \text{and } Z=Z'$$

$$\text{if } |M_3| \geq |M_2| \quad , \quad M = M_3 \quad \text{and } Z=Z''$$

The Doppler algorithm consists of calculating Z and finding α, where

$$\alpha = \sin^{-1} Z \tag{4.13}$$

Then the expression for the error in Z is

$$|\Delta Z| \leq \left| \frac{1/2 + \sin|\alpha|}{M} \right| \tag{4.14}$$

The question arises: what is the smallest value for the magnitude of M as a function of α? This question is considered in Appendix III, with the result

$$|M| \geq \left| A \sin(\pi/4 - |\tfrac{\alpha}{2}|) \right|$$

Then equation (4.14) is rewritten

$$|\Delta Z| \leq \left| \frac{1/2 + \sin|\alpha|}{A \sin(\pi/4 - |\frac{\alpha}{2}|)} \right| \tag{4.15}$$

The velocity of a reflector relative to the transmitter is related to the Doppler shift by

$$v = \frac{\omega\lambda}{4\pi} = \frac{\alpha\lambda}{4\pi\ \Delta t} \tag{4.16}$$

Then errors in velocity are related to errors in Doppler angle by

$$\Delta v = \frac{\Delta\alpha}{\alpha} v \tag{4.17}$$

The quantity $\Delta\alpha$ is gotten by differentiating equation (4.13)

$$d\alpha = \frac{1}{\sqrt{1-Z^2}}\, dZ \tag{4.18}$$

But $Z = \sin\alpha$, so

$$\Delta\alpha = \frac{\Delta Z}{\cos\alpha} \tag{4.19}$$

$$|\Delta\alpha| \leq \left| \frac{1/2 + \sin|\alpha|}{A\ \sin(\pi/4|\frac{\alpha}{2}|)\ \cos\alpha} \right| \tag{4.20}$$

$$\leq f(\alpha)$$

$$|\Delta v| \leq \left| \frac{f(\alpha)}{\alpha} \right| \tag{4.21}$$

Inspection of equation (4.20) reveals that $f(\alpha)$ is a monotonically increasing function; α^{-1} is monotonically decreasing. Then $f(\alpha)\ \alpha^{-1}$ has a minimum (Figure 4.2). Numerical evaluation of this function shows that this minimum occurs for $\alpha = .446$ radians.

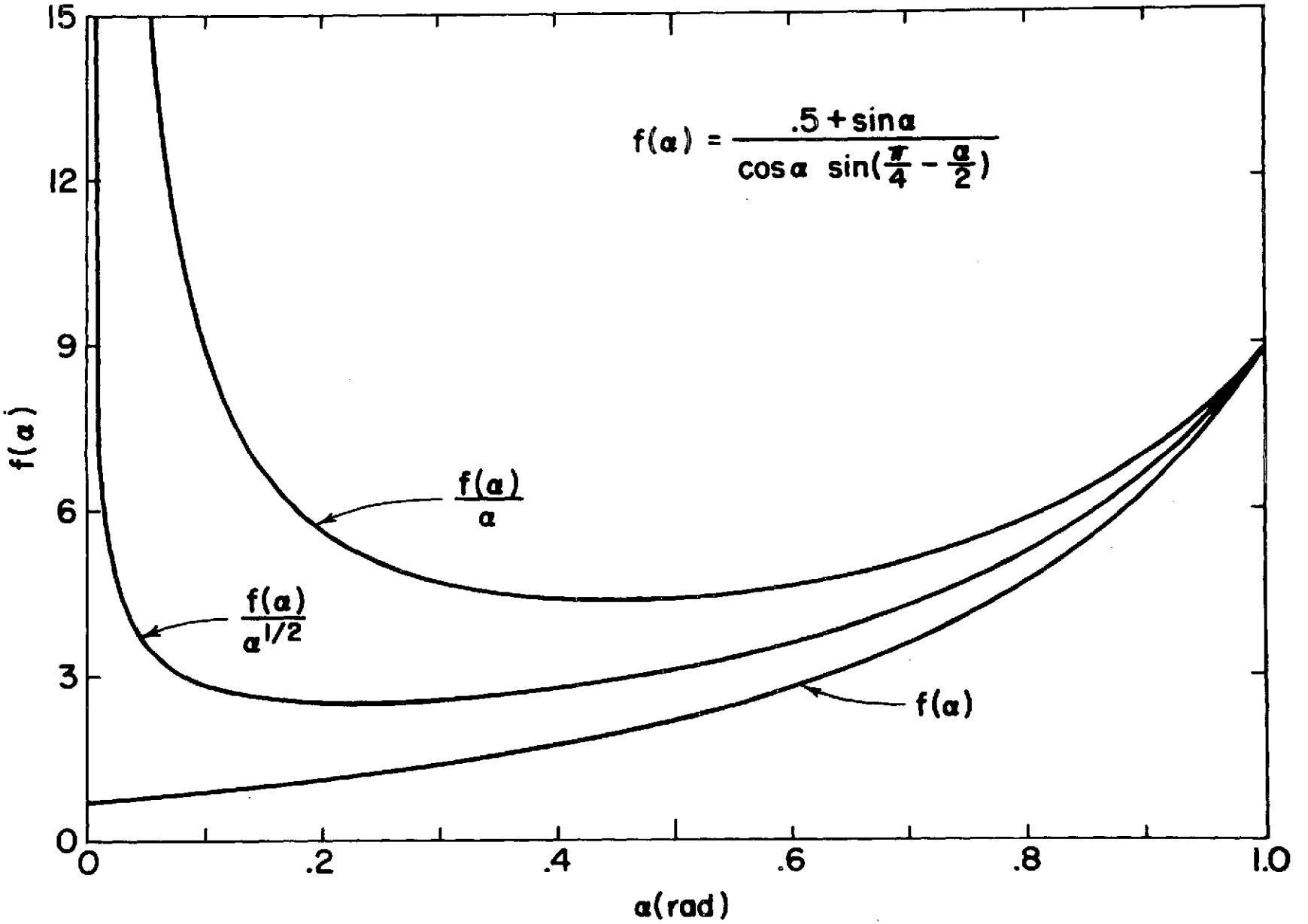

Figure 4.2. Variations of functions of α.

From the definition $\alpha = \omega \Delta t$, the optimal technique for measuring ω seems to be to vary Δt, the time between transmitted pulses, until $\alpha = .446$. Then $\omega = .446/\Delta t$. This method is impractical because the lifetime of a meteor trail is finite. For low velocities, Δt may become larger than the trail lifetime. A practical approach is to choose Δt such that $\alpha = .446$ for the maximum velocity of interest. Since this maximum velocity is about 100 $msec^{-1}$,

$$v_{max} = \frac{\omega_{max} \lambda}{4\pi}$$

$$\omega_{max} = \frac{100 \cdot 4\pi}{7.33} = 171.4 \text{ rad. sec}^{-1} .$$

Then $$\alpha = \omega_{max} \Delta t$$

$$\Delta t = \frac{.446}{171.4} = 2.602 \text{ msec}$$

The optimum pulse-repetition frequency for a single measurement of Doppler frequency is then 384 Hz. If more than one measurement is to be taken, another factor must be considered. For any given reflector lifetime, the number of measurements that can be taken is proportional to the PRF. The improvement in accuracy of a measurement due to data averaging is proportional to the square root of the number of values averaged. Equation (4.21) is modified to

$$\Delta v' \sim \frac{f(\alpha)}{\alpha} \cdot \frac{v}{\sqrt{PRF}} \qquad (4.22)$$

But α is inversely related to the PRF, so that

$$\Delta v' \sim \frac{f(\alpha)}{\alpha} v\ \alpha^{1/2}$$

$$\Delta v' \sim f(\alpha)\ \alpha^{-1/2}\ v \qquad (4.23)$$

When the quantity $f(\alpha)\alpha^{-1/2}$ is plotted, the minimum occurs for α = .227 rad (Figure 4.2). Following the procedure used for the single measurement case, the optimum PRF is 755 Hz. It is important to note that the function $f(\alpha)\alpha^{-1/2}$ is fairly flat near the minimum. The implication is that the advantage gained by multiple measurement is very nearly cancelled by the loss in accuracy due to a higher PRF. One concludes that any PRF in the range 400-1700 Hz, corresponding to α in the range .1-.4 rad, is acceptable.

The single-measurement accuracy is calculated using the following parameters:

$$v = 100 \text{ msec}^{-1}$$

$$\text{PRF} = 400 \text{ Hz}$$

$$\omega = \frac{4\pi v}{\lambda} = 171.4 \text{ rad. sec}^{-1}$$

$$\alpha = \omega \Delta t = .4285 \text{ rad}$$

$$|\Delta v| \leq \frac{f(.4285)}{.4285} \cdot 100$$

$$\leq \frac{435}{A}$$

Since A, the signal amplitude, can range from 0-511, a reasonable value is 100. Then $|\Delta v| < 4.85 \text{ msec}^{-1}$.

4.3 *Phase Comparison*

In order to calculate angles of arrival, phase comparisons between pairs of separate antenna-receiver sets must be made. Such phase comparisons are required for measurement of coarse elevation, fine elevation, and azimuth angles. The phase-comparison problem can be easily understood in the light of the following analogy: given two clocks which cannot be viewed simultaneously; how can their indicated times be compared? If one observes the first, and then, a moment later, observes the second, both clocks have moved forward by some time increment. Obviously, one must use a stopwatch in order to know the displacement which occurred between observations. In the case of meteor radar, clocks one and two correspond to phase at two receivers. The phases cannot be observed simultaneously because receiver outputs are multiplexed sequentially (Section 3.3). The required "stopwatch" is simply the Doppler frequency; the phase increment between measurements is the Doppler frequency multiplied by the time increment between measurements. This quantity is α, the Doppler angle, as defined in Section 4.2.

The phase comparison requires the following sequential measurements:

1. Sine output of Receiver #1
2. Cosine output of Receiver #1
3. Sine output of Receiver #2
4. Cosine output of Receiver #2

From the above analogy it appears that there should be some way to use these four quantities, together with Doppler frequency and time between measurements, for a calculation of phase difference. Such a calculation is outlined in Appendix IV.

Singularities in this calculation can only occur when all four measurements return the value zero. This case is possible only when

$$\omega\Delta t = \pi/2$$

ω = Doppler frequency

Δt = pulse-repetition period

Since both the sine and cosine of the phase difference are given by the calculation, phase differences can always be calculated within ambiguities of multiples of 2π radians. This ambiguity is eliminated by antenna placement.

Accuracy of the phase-difference measurements is, to a first order, the same as the accuracy of measurements of the Doppler angle as defined in Section 4.2. For this reason, phase-difference measurement is accurate to at least within .03 radians.

4.4 *Angles of Arrival*

In the Illinois meteor-wind system, the angles of arrival of an echo are obtained using four spaced receiving antennas in an interferometric mode. To determine the angles of arrival, the phase differences between pairs of antennas are measured. The symbols θ_{ij} and d_{ij} are used to represent the phase difference and ground distance between antennas A_i and A_j. Then the phase differences of interest are written (see Figures 3.1 and 3.5)

$$\phi_{12} = \frac{2\pi\, d_{12}}{\lambda} \cos\zeta \cos\psi \qquad (4.24)$$

$$\phi_{41} = \frac{2\pi\ d_{41}}{\lambda} \cos\zeta\ \cos\psi \tag{4.25}$$

$$\phi_{13} = \frac{2\pi\ d_{13}}{\lambda} \cos\zeta\ \sin\psi \tag{4.26}$$

where ζ and ψ are the elevation and azimuth angles of arrival, and λ the radar wavelength. Phase differences ϕ_{12} and ϕ_{41} are taken from antennas aligned along the beam axis. Distances d_{12} and d_{41} are 1λ and 20λ, respectively. These two phase differences are used to find the elevation phase difference, with the widely spaced antenna pair acting as a vernier to refine the phase difference determined by the closely spaced pair. The azimuth phase difference is simply ϕ_{13}, which is taken from the antenna pair spaced one wavelength, and oriented perpendicular to the beam axis.

Two quantities, P_{el} and P_{az}, are defined as

$$P_{el} = \frac{\phi'_{41}}{2\pi\ d_{41}} \tag{4.27}$$

$$P_{az} = \frac{\phi_{31}}{2\pi\ d_{31}} \tag{4.28}$$

where ϕ'_{41} is the refined version of ϕ_{41}. Then P_{el} and P_{az} are the normalized phase differences for the elevation and azimuth antenna pairs;

$$P_{el} = \cos\zeta\ \cos\psi \tag{4.29}$$

$$P_{az} = \cos\zeta\ \sin\psi \tag{4.30}$$

The angles of arrival are gotten from trigonometric manipulations of P_{az} and P_{el}:

$$\frac{P_{az}}{P_{el}} = \tan\psi$$

$$\psi = \tan^{-1}\left(\frac{P_{az}}{P_{el}}\right) \tag{4.31}$$

$$P_{az}^{2} + P_{el}^{2} = \cos^{2}\zeta$$

$$\zeta = \cos^{-1}(P_{az}^{2} + P_{el}^{2})^{1/2} \tag{4.32}$$

The angles of arrival algorithm is a three-step procedure. First, the wide-spaced elevation phase data are used to refine the close-spaced elevation phase information. Next, the elevation and azimuth phase differences are normalized. Finally, the normalized phase differences are combined to yield the azimuth and elevation angles of arrival.

5. DATA REDUCTION SUBSYSTEM CODING AND SIMULATION TESTING

The data-reduction subsystem contains all the measurement algorithms, and operates on the reduced frames produced by the echo-search subsystem. In order to verify the proper operation of the measurement algorithms, a simulation of the hardware and software subsystems up to data reduction is done. That is, a simulation program is used which, given as input data the parameters that describe a meteor-trail echo, produces a reduced frame. These descriptive parameters include the coordinates and velocity of the specular point, and also the amplitude of the echo signal and noise at the receiver output. The reduced frames produced by simulation are input to the reduction system, and the coordinates and velocity output by the reduction system are compared to the echo parameters initially given to the simulation program. The simulation is used to test the data-reduction subsystem on a comprehensive set of parameters which include all of the expected characteristics of meteor-trail echoes. In this way, algorithm validity is demonstrated, and the minimum signal-to-noise ratio which gives the required measurement accuracies is determined.

Data-reduction subsystem testing is done in three steps. First, the measurement algorithms are used to design the data-reduction program. Next, the program for simulating the meteor-radar system up to the data-reduction subsystem is written. Finally, the actual testing is done. Each step is described in detail in the following paragraphs.

5.1 *Subsystem Coding*

The data-reduction subsystem consists of 6 subroutines, 4 Common Blocks, and 2 Block Data programs. Each subroutine performs a single operation on the data stream. Three of the Common Blocks are used for communications

between subroutines; the fourth block contains data related to the spacing between antennas. The six subroutines which perform the data reduction are described here; listings are given in Appendix V.

SDRIV1 is the interface between the reduced frames input to the reduction system, and the subroutines containing measurement algorithms. It organizes the data for use by the measurement subroutines. Each of the other subroutines is subject to certain error conditions, which can occur with a noisy echo or a very high Doppler shift. These error conditions are sensed within the measurement subroutines, and communicated to SDRIV1 through one of the common blocks.

SDRIV1 groups the input data and calls the various measurement subroutines in the proper order. If no error is sensed in any of the measurement subroutines, SDRIV1 outputs the measured quantities; otherwise, an appropriate error message is printed indicating the nature of the error.

DOPPLER is the implementation of the Doppler algorithm. Elements taken from four of the phase lines are its arguments, and $\sin\alpha$ is its output. One error condition exists. If both the second and third arguments are zero, no calculation can be done. That is, if both M_2 and M_3 are zero from Section 4.2, an error condition occurs. This error is flagged as error 21.

SINCOS takes $\sin\alpha$, the output of DOPPLER, and generates the sine and cosine of multiples of α as well as α itself. The sine and cosine of multiples of α are needed by the phase-difference algorithm. The quantity α is needed for determination of the radial velocity. An error occurs if the input quantity $\sin\alpha$ has magnitude greater than unity. This condition is flagged as error 41.

ANGLES changes the sine and cosine data from pairs of receivers into their phase difference. The sine and cosine of this phase difference are first calculated, using the four arguments and the data generated by SINCOS. Error 11 occurs if both the calculated sine and cosine are zero; otherwise, the sine and cosine of the phase difference are used to find the phase difference in the region $-\pi$ to π.

ARRIVL uses the phase differences between pairs of antennas and the antenna spacing data to find the angles of arrival. Two error conditions exist. If the phase differences between both the azimuth and elevation antenna pairs are zero, error 31 is flagged. The subroutine calculates the cosine of the elevation angle, and then generates the elevation angle itself. If the cosine of the elevation angle is greater than unity, error 32 occurs.

TRGINV takes the sine and cosine of an angle as input, and returns the angle itself in radians. The returned angle is in the range $-\pi$ to π.

Table 5.1 illustrates the interaction of the data-processing subroutines. Before a change is made in any of the six programs, the effect on all other programs must be considered.

Four Common Blocks are used by the processing system to store the hardware system and echo parameters. Block DIST contains data related to the distances between the antennas. This data is used by the program ARRIVL. The block holds the reciprocals of the antenna spacings, divided by 2π, since this is the form of the spacing data required by ARRIVL. Also, the reciprocal of the distance between the widely-spaced antenna pair, half of the reciprocal of this distance, and the distance itself are

Table 5.1

Data processing subprogram interaction

Program Name	Called By	Required Subroutines
SDRIV1	—	ANGLES ARRIVL DOPPLR SINCOS
ANGLES	SDRIV1	TRGINV
ARRIVL	SDRIV1	TRGINV
DOPPLR	SDRIV1	—
SINCOS	SDRIV1	TRGINV
TRGINV	ANGLES ARRIVL SINCOS	—

stored for use by ARRIVL. The six values stored in DIST are initialized by a block-data program named SPCING. Once initialized, the values are not changed. Block ERROR is a single word used for communicating error conditions between the measurement subroutines and SDRIV1. It is initially set to zero, indicating no error, by the block-data program ERROR. Block TRIG holds the sine and cosine of α, 2α, and 3α, as well as α itself. It is used for communication between the programs SINCOS and ANGLES. Block AOFA holds the angles of arrival. The block is written by the program ARRIVL, and read by SDRIV1. Table 5.2 illustrates how these various blocks are used for communication.

5.2 *Simulation Program*

There are two sources of noise in the system. First there is sky noise. This noise is Gaussian distributed, and characterized by a standard deviation. It is additive with the echo signal at the receiving antennas. The second noise source is quantization by the A/D converter. This noise is uniformly distributed on the interval [0, 1). Since the A/D converter operates on the received signal, quantization occurs on the sum of the received echo and the sky noise. The simulation takes into account these noise sources by modeling the signal flow through the system. The echo signal itself is created first. Then, Gaussian noise is added to the signal. Finally, the signal is quantized. Echo signal creation requires two sets of parameters: the antenna-spacing data, and the echo parameters. The spacing data is simply the distance between the antennas in wavelengths. The relative antenna placement shown in Figure 3.1 is assumed. The distances between antennas shown in Figure 3.1 are suggested; the actual distances may vary by a few percent without any adverse effect.

Table 5.2

Data processing subsystem common block usage

Block Name	Initializing Program	Written into by	Read by
AOFA	—	ARRIVL	ARRIVL SDRIV1
DIST	SPCING	—	ARRIVL
ERROR	ERROR	ANGLES DOPPLER ARRIVL SINCOS	SDRIV1
TRIG	—	SINCOS	ANGLES SDRIV1

The spacing data used in the processing system are the actual measured values, rather than the proposed distances. The echo parameters include the azimuth angle, elevation angle, velocity, and amplitude of the reflecting point. With this data, the phase differences between signals at the various antennas and the Doppler shift of the received signals can be calculated. The processing system deduces Doppler shift and velocity from the phase change per pulse repetition period of the signal at any antenna. The simulation assumes a PRF of 400 Hz and a radar wavelength of 7.33 m, in order to calculate the phase change due to Doppler shift.

One other factor is required before the echo signal is created: the absolute phase at any one of the receivers. Recall that the angles of arrival are derived from phase differences between antennas, and Doppler shift from phase change with time. But from Section 4, it is apparent that algorithm accuracies are functions of the absolute phase. The simulation takes as an input parameter the number of trials to be performed, as well as the echo characteristics. Starting with an absolute phase of zero at antenna one for the first trial, the absolute phase for each successive trial is that of the previous trial incremented by $2\pi/M$, where M is the total number of trials. The processing system results for each trial are compiled; after the final trial, the average and standard deviation for the azimuth angle, elevation angle, and velocity returned by the processing system are output. In this way, the effect of absolute phase on measurement accuracy is included in the overall accuracy determination.

Six quantities specify the characteristics of an echo. These quantities are input from the keyboard, and used to construct a series of reduced data frames. The first quantity input is the echo amplitude. This quantity is specified in terms of the A/D converter output scaling, and can vary from zero to 511. It controls the effect of quantization noise on processing accuracy, in that the created echoes are scaled to this amplitude, and then truncated to an integer value. The second quantity input is the standard deviation of the Gaussian noise which is to be added to the echo signal. This quantity is also specified in terms of A/D converter scaling. Signal-to-noise ratio is set through both the amplitude and noise specification. For 20 dB S/N, amplitude may be set at 100 and noise at 10 units. The third and fourth quantities input are the azimuth and elevation angles of arrival in radians; the fifth is the radial velocity of the reflecting point towards or away from the receiving array. The last quantity input is the number of trials to be performed with the same echo parameters. After the last quantity is input, the simulation and processing begins. The specified number of trials is made, each with different initial phase, and different random values of Gaussian additive noise. The results of the test are printed, and the simulation program is ready for a new test specification. A listing of the simulation program is given in Appendix V. A sample run is shown in Table 5.3.

5.3 *Simulation Results*

The simulation testing is actually two independent test series. The first series verifies the correct operation of the processing system under no-noise conditions, and determines the range of values of the echo parameters for which the processing system produces the required results.

Table 5.3

Sample runs of the TRY4 simulation program

```
************************************
AMPLITUDE(1 TO 500)
>100
NOISE STAND.DEV.
>2
ELEVATION ANGLE (RAD)
>.7854
ANGLE WITH DUE NORTH (RAD)
>.2
RADIAL VELOCITY (M/S)
>20
NO. OF ITERATIONS
>29
            AVERAGE       STANDARD DEV
AZIMUTH      0.2002          0.0085
ELEVATION    0.7853          0.0021
VELOCITY    20.5373          2.3077
************************************
AMPLITUDE(1 TO 500)
>100
NOISE STAND.DEV.
>2
ELEVATION ANGLE (RAD)
>.7854
ANGLE WITH DUE NORTH (RAD)
>.2
RADIAL VELOCITY (M/S)
>50\\20
NO. OF ITERATIONS
>29
            AVERAGE       STANDARD DEV
AZIMUTH      0.2003          0.0073
ELEVATION    0.7853          0.0018
VELOCITY    20.2524          2.2158
```

The second series determines the measurement accuracies of the processing system when additive Gaussian noise is present, and finds the minimum signal-to-noise ratio for which the required measurement accuracies are achieved.

5.3.1 *Validity test.* In order to test the validity of the processing system, a parameter list is given to the simulation program, which then produces a reduced frame. This reduced frame is passed to the processing system, which attempts to recover the input parameters. For the validity test series, zero Gaussian additive noise is used; however, quantization noise is present. Therefore, the parameters input are never recovered exactly. The criteria used for identifying a processing system failure is the following: if any of the recovered parameters vary by more than just a few percent from the input parameters, a failure has occurred. Using this definition, the input parameters are varied throughout their expected range, and the validity region is delineated by the input parameter values for which processing system errors occur. In mapping this region, a standard input parameter list is used. Each parameter in the list is varied independently until a processing system error occurs. The points of error are noted, and then that parameter is returned to its standard value, and another parameter is varied. This process is continued until the validity region is completely determined. The standard parameter list is as follows:

Azimuth Angle	:	11°
Elevation Angle	:	45°
Velocity	:	50 $msec^{-1}$
Amplitude	:	100

These parameters are selected in view of the transmitting and receiving antenna patterns from Section 3, and the meteor-trail characteristics from Section 2. They represent typical operating parameters, rather than the optimal conditions for the processing system. The amplitude of 100 sets the quantization noise at less than one part in 100, as described in preceding paragraphs.

Test results show the validity region for elevation angle to be 0 to 90°. The error in measurement of this quantity is relatively constant from 0 to 70°, but rises sharply above 70°. The required validity region is 0 to 90°, so that satisfactory performance is achieved. For azimuth angle, the validity region is -45° to 45°. According to the specification in Section 2, the required region is -90° to 90°. The equations in Section 4.4 indicate that the validity region cannot be increased without decreasing the azimuth antenna pair spacing from its current dimension of one radar wavelength. The error in azimuth angle measurement is nearly constant across the validity region. The velocity measurement is valid from -300 to 300 $msec^{-1}$. The measurement error is constant for wind magnitudes under 100 $msec^{-1}$, but grows for wind magnitudes greater than 100 $msec^{-1}$. This is the expected result, as indicated in Section 4.2. The processing system satisfies all of the measurement region requirements, except for azimuth. A discussion of methods for increasing the azimuth validity region is given in Section 6.

5.3.2 *Noise test.* In order to find the minimum signal-to-noise ratio (S/N) for which the required measurement accuracies are achieved, a series of tests is conducted. Again, a standard parameter list is used, with the following values chosen:

Azimuth angle	11°
Elevation angle	45°
Amplitude	100°

These parameters are held constant throughout the test series. The velocity and Gaussian-additive noise are varied, and the test results tabulated. In a preliminary test series, measurement accuracy was found to depend on velocity magnitude but not direction. The values of velocity used in the test series are, therefore, chosen as 0, 10, 20, 50, 100, and 200 $msec^{-1}$. The Gaussian-additive noise values used in the test series are 1, 2, 5, 10, and 20 units. Since the amplitude is set at 100 units, the corresponding S/N are 40, 34, 26, 20, and 14 dB. With 6 values for velocity and 5 for additive noise, a total of 30 tests are made. Each test consists of 29 trials. The average and standard deviation of azimuth, elevation, and velocity for each set of trials are the outputs of each test.

For all tests, the averages agree closely with the input parameters. The standard deviations of the output quantities increase with increasing additive noise. Figures 5.1, 5.2, and 5.3 show the standard deviations of the velocity, elevation, and azimuth measurements as a function of additive noise for various velocities. Note that the curves on all three figures are indistinct for velocities less than or equal to 100 $msec^{-1}$. This supports the previous conclusion that velocities below 100 $msec^{-1}$ do not affect measurement accuracy. The curves on all three figures show a marked increase in error for a velocity of 200 $msec^{-1}$, however.

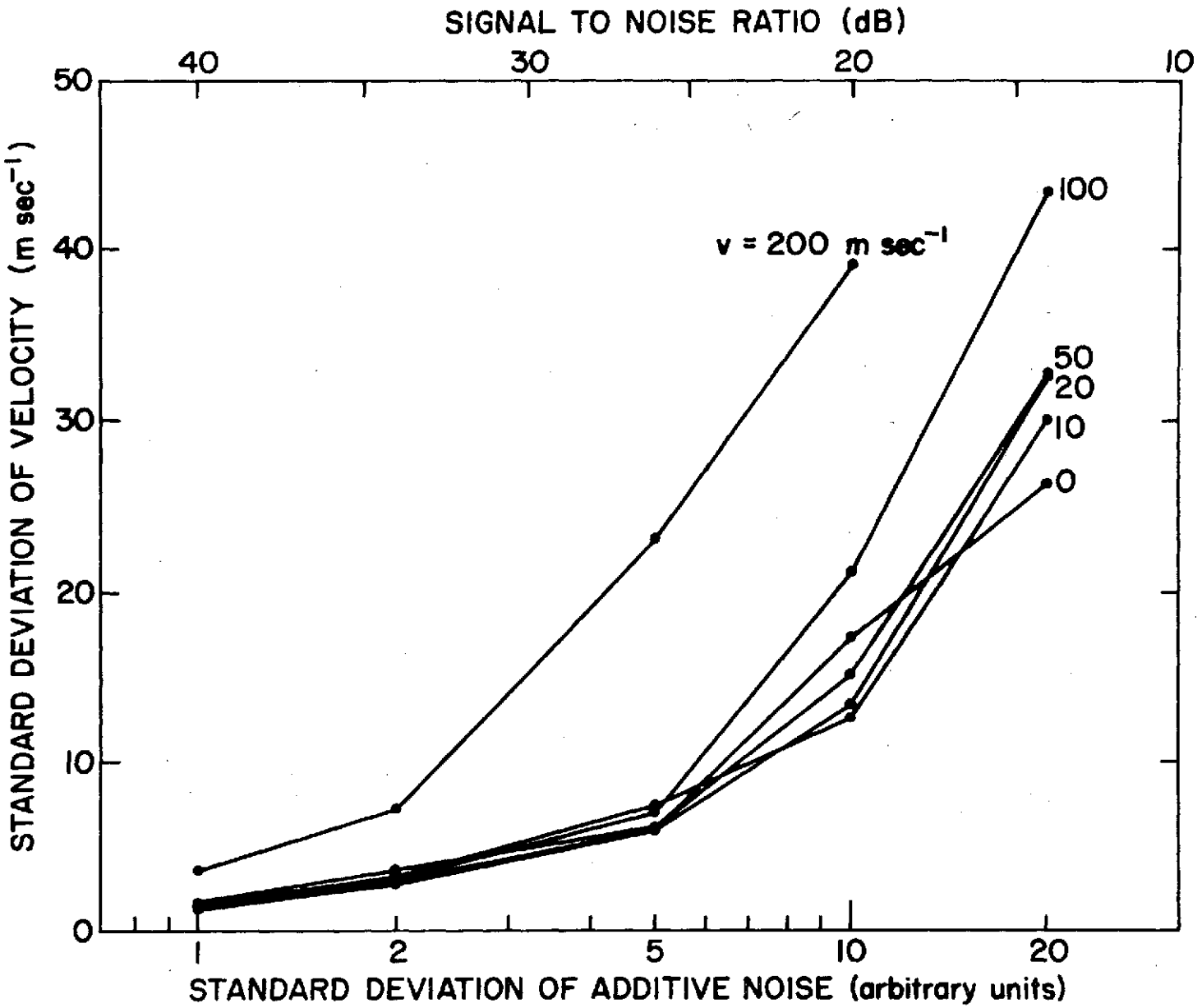

Figure 5.1. Velocity standard deviation versus additive noise.

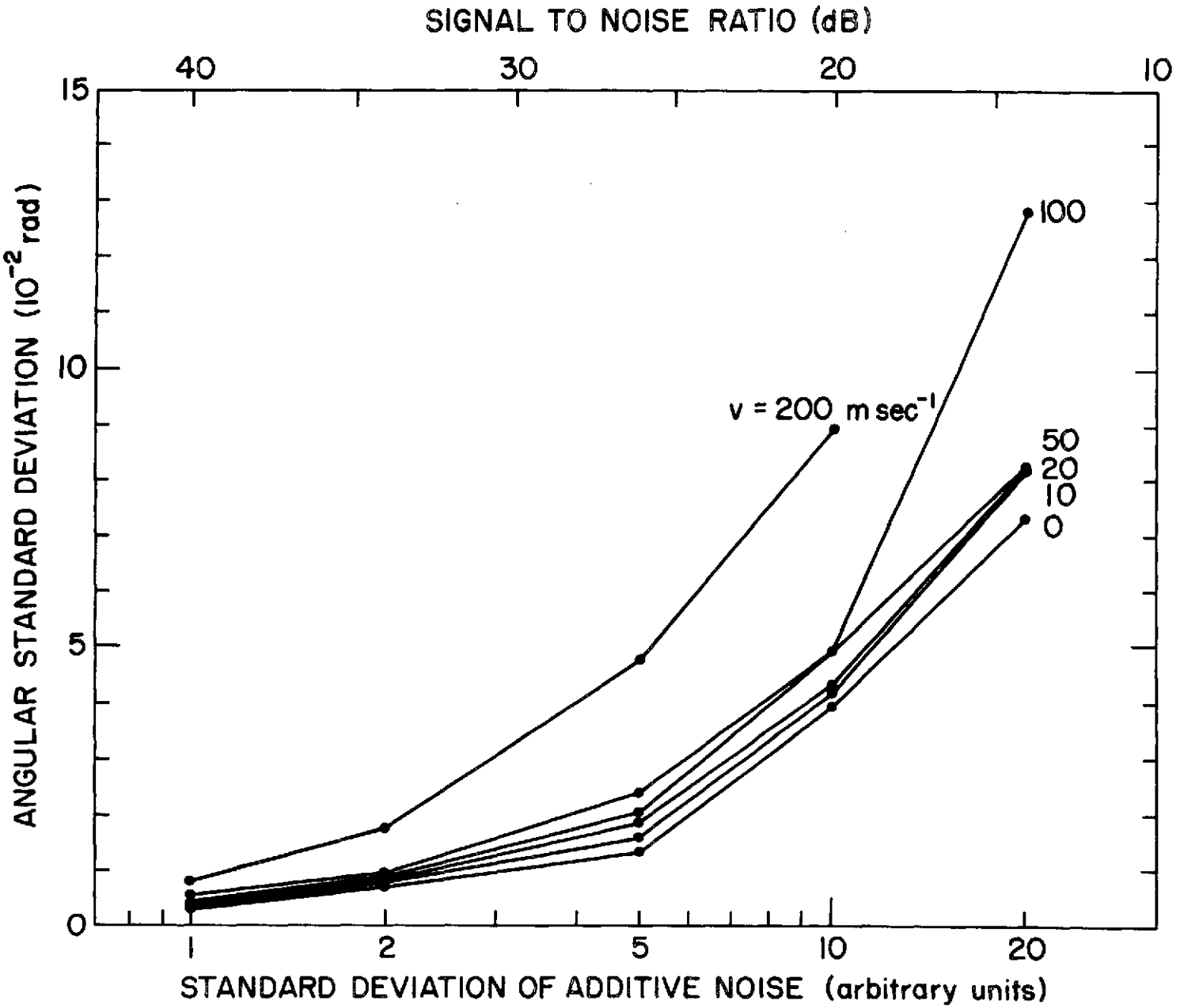

Figure 5.2. Azimuth standard deviation versus additive noise.

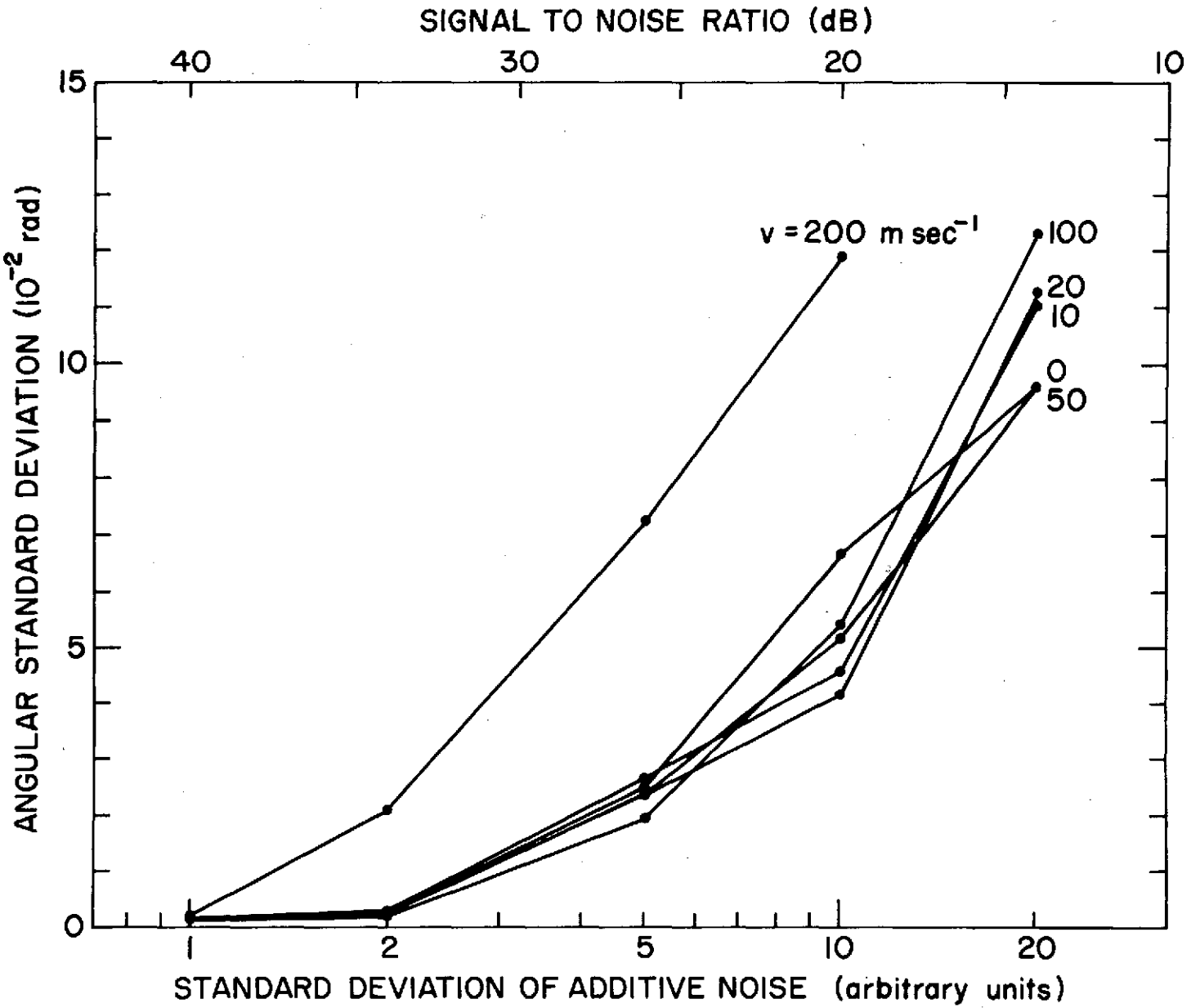

Figure 5.3. Elevation standard deviation versus additive noise.

The minimum S/N which gives the required measurement accuracies is found by considering the 100 $msec^{-1}$ curve on each figure. From Section 2, the velocity accuracy requirement is 5 $msec^{-1}$. Figure 5.1 indicates that a S/N of 30 dB gives this result. The required elevation accuracy is .003 rad; from Figure 5.2, 33 dB gives this result. Finally, the azimuth accuracy requirement is .1 rad, which is achieved for a S/N of 17 dB. Obviously, the elevation angle is the most critical.

From Section 1, the highest the S/N can ever be is 40 dB. The 33-dB requirement is under this 40-dB limit, and is, therefore, achievable. With 33-dB S/N, velocity accuracy is 4 $msec^{-1}$ and azimuth accuracy .01 rad. Then all requirements are met by a signal-to-noise ratio of 33 dB.

6. RESULTS AND SUGGESTIONS FOR FUTURE WORK

In preceding chapters, the hardware and software subsystems which make up the meteor-radar system are described. Two points are addressed in the following subsections. First, what combination of pulse width, PRF, and receiver bandwidth is optimal for the total system. Second, how can the azimuth validity region be increased. In the last subsection, conclusions and suggestions for future work are presented.

6.1 *Pulse Width, Bandwidth, and PRF Tradeoffs*

The system hardware and measurement algorithms place constraints on three system parameters: transmitted pulse width, PRF, and receiver bandwidth. These constraints are considered individually in previous sections. Here, all constraints are brought together, tradeoffs are evaluated, and the final parameter selection is made.

The transmitter is rated for a nominal average power of 20 kw, and a maximum average power of 40 kw. The instantaneous power is fixed at 5 Mw. The effect of fixing the average and peak powers is to impose an inverse relation between pulse width and PRF. The products of PRF and 3-dB pulse width are constrained to .004 for nominal power operation, and .008 for maximum power operation.

Two range algorithms are given in Section 4.1. One uses a ratio method, the other a parabola method. The parabola method requires a characteristic pulse at the receiver output wider than 30 μsec at 20-dB points (as opposed to the 20-μsec requirement of the ratio method) but gives a more accurate range determination than the ratio method, and is used in the system. For a Gaussian pulse, 30-μsec wide at 20-dB points, the 3-dB width

is 12 μsec. With multiple targets, however, the narrower the characteristic pulse, the better the resolving power of the radar system. The characteristic pulse width is then 12 μsec, and no wider, so that the range algorithm requirement is satisfied, and the resolving power is not compromised.

In passing through a finite-bandwidth receiver, the shape of an input pulse is modified according to the relations given in Section 4.1. Relative to an infinite-bandwidth receiver, the output pulse length is increased, and the amplitude decreased. The range-algorithm pulse-width constraint applies to the receiver output, rather than the input. In order to minimize the signal amplitude loss in the receiver, a bandwidth which decreases the signal by no more than 5 percent is needed. Solving equations (4.3) and (4.4) (using a characteristic pulse width of 12 μsec) the required receiver bandwidth and transmitted pulse width are 88 kHz and 11.4 μsec.

The Doppler algorithm gives good results for a PRF in the range 400-1600 Hz, with optimal results at 700 Hz. From the system interconnection plan in Section 3, however, the highest usable PRF is 625 Hz; any higher PRF causes range ambiguities. Then the acceptable range for the PRF is 400-625 Hz.

Using 400 Hz and 11.4 μsec as the PRF and transmitted pulse width, the average transmitted power is 23 kw, very nearly the nominal power rating. Increasing the PRF to 625 Hz brings the average power to 36 kw.

A PRF, pulse width and bandwidth of 400 Hz, 11.4 μsec, and 88 KHz are reasonable parameters to use initially. Of course, the assumptions of Gaussian receiver bandpass and transmitted pulse shape are only approximations. The transmitted pulse width may require some stretching

or shrinking in order to get a receiver output pulse 30 μsec wide at 20-dB points. Once the transmitter is completely operational, the PRF can be increased to 625 Hz. At that point, increasing the PRF or pulse width will degrade system performance by introducing range ambiguities and increasing the likelihood of multiple-echo overlap.

6.2 *Azimuth Validity Region*

With the antenna arrangement of Figure 3.1, the azimuth validity region is from -45° to 45° relative to due north. The specifications from Section 2 call for the region to extend from -90° to 90°. Although few echoes are expected from outside the main transmitter beam, which extends from -26° to 26°, some means for identifying out-of-beam echoes is needed. Several methods to achieve this identification are given below.

If the azimuth antenna spacing is decreased to $\lambda/2$, the validity region becomes -90° to 90°. This straightforward solution is difficult to implement, however, because of mechanical and electrical interference problems with such a closely spaced antenna pair. Even the current 1λ spacing is perhaps closer than desirable. This solution therefore cannot be used.

Another available solution uses the high directivity of the Yagi antenna azimuth pattern to identify out-of-beam echoes. The azimuth antenna pair phase-center spacing is maintained, but the Yagi antennas which form the pair are skewed from due north by a half-beamwidth, one to the left and the other to the right. Then echoes which are in the main beam of both antennas are from the desired region. Echoes outside this region are identified by the signal amplitude differential between the left-pointing and right-pointing antennas. The main difficulty with

this approach is in locating the phase center of the Yagi. Very little published information is available on this topic. Another problem is the gain-match required of the two receivers connected to the azimuth pair antennas. Although difficulties arise in implementing this solution, it is a practical technique for recognizing out-of-beam echoes.

A third solution adds a dipole antenna to the receiving array. Echoes out-side the main beam are recognized by the relative strengths of the signals from a Yagi and dipole. Much stronger signals are available at the Yagi than the dipole for echoes in the main Yagi beam. Outside the beam the signals from a Yagi and dipole are nearly the same. This solution is essentially similar to the previous one, but avoids the Yagi-phase-center problem. However, extra multiplexer channels are needed, or the multiplexing sequence must be modified, in order to add the additional information from the dipole to the frame.

The azimuth ambiguity problem indicates that more work is needed in the area of the receiving array design; perhaps a completely new antenna arrangement is needed. The best approach to the problem of antenna array design at this point is to implement a portion of the receiving array, and determine the extent of array modification needed to satisfy the system requirements.

6.3 *Suggestions for Future Work and Conclusions*

In previous Sections, the hardware and software subsystems required to build a meteor-wind system for observing short-period dynamics are described. The system is built around a medium-scale computer; all meteor-echo recognition and parameter measurement algorithms are incorporated in software. The computer eliminates many complicated hardware components,

which results in an increased mean-time between failures. All meteor-echo parameters are measured to the required accuracy for observing gravity waves; in particular, a height accuracy of ±1 km is achieved. The system uses a high-power transmitter and a high-speed collection system to achieve temporal as well as spatial resolution.

The problem of azimuth-angle ambiguities for echos outside the main lobe of the transmitting antenna requires more study. In fact, the entire receiving-antenna array should be reevaluated, with the intent of finding an arrangement of antennas which has no azimuth or elevation angle ambiguities. With such an arrangement, an all-sky system is available by simply replacing the high-directivity transmitting and receiving antennas with dipoles. The software system is modular, so that a different receiving array requires only minor modifications to the system programs.

System calibration is also an important, unresolved problem. Such things as cable delays and receiver signal delays must be calibrated out of the system. One method for calibration uses the known path of satellites. The radar system tracks the satellite, and the known path of the satellite is compared to the path given by the radar system. Another approach uses a low-power transmitter suspended from a balloon. The balloon is released north of the receiving array, so that it rises through the antenna boresight. The transmitter is tracked by the receiving system, as well as by a theodolite. The optical measurement is used to calibrate the radar measurement. Both these methods are reasonable approaches to the initial calibration problem; however, they are not suitable for use on a routine basis.

Although 9 channels of useful data are available at the receivers during echo reception, only one channel can be digitized at a time. A method for sampling all channels simultaneously during echo reception would simplify the data reduction subsystems, and also increase the useful information gotten from each meteor trail. With the addition of some hardware, the radar system can operate in this mode. The video channel is digitized continuously, until a meteor-trail echo is detected. Then, under program control, the digital input/output interface to the computer is used to output the time in μsec after pulse transmission when the next echo is expected. A counter, driven by a 1 MHz clock, is reset to zero as the next pulse is transmitted. A comparator senses when the count equals the expected delay in μsec; sample-and-hold circuits connected to each of the eight phase-comparator channels are strobed at that instant. The A/D converter is then used to serially input the 8 samples. The total hardware required for this mode consists of a counter, comparator, and 8 sample-and-hold circuits. The 1 MHz clock signal is available from the A/D converter. Since the required hardware is mainly digital integrated circuits, the physical volume and interconnection complexity are low. The addition of this small amount of hardware replaces a large amount of software, and results in more data collected per transmitted pulse. Modifying the system in this way may prove useful, once the basic system is operational.

Ground-based measurements of short-period wind variabilities in the meteor region are essential to the investigation of atmospheric dynamics. The system described in previous chapters should give a higher

echo rate and better resolution than any meteor-wind system currently available, and contribute significantly to the understanding of atmospheric winds.

LIST OF REFERENCES

Barnes, A. A., Jr. (1968), Winds and Densities from Radar Meteor Trail Returns, 80-120 km, *Met. Monog., 9,* 190-195.

Barnes, A. A., Jr. (1972), Using VHF Radars to Probe the Atmosphere, *15th Radar Meteorology Conf.,* 341-352.

Beer, T. (1972), Atmospheric Waves and the Ionosphere, *Contemp. Phys., 13,* 247-271.

Blamont, J. E. and C. deJager (1961), Upper Atmospheric Turbulence near the 100 km Level,*Ann. Geophys., 17,* 134.

Booker, H. G. (1956), Turbulence in the Ionosphere with Applications to Meteor Trails, Radio Star Scintillation, Auroral Echoes, and other Phenomena, *J. Geophys. Res., 61,* 673.

Bowles, K. L. (1959), Symposium on Fluid Mechanics in the Ionosphere, *J. Geophys. Res., 64,* 2071.

Georges, T. M. (1967), Ionospheric Effects of Atmospheric Waves, *ESSA, Tech. Report IER 57 - ITSA, 54.*

Greenhow, J. S. (1959), Eddy Diffusion and its Effect on Meteor Trails, *J. Geophys. Res., 64,* 2208.

Greenhow, J. S. and Nuefeld, E. E. (1956), The Height Variation of Upper Atmospheric Winds, *Phil. Mag., 1,* 1157.

Greenhow, J. S. and Nuefeld, E. E. (1959), Measurement of Turbulence in the 80 to 100 km Regions from the Radio Echo Observations of Meteors, *J. Geophys. Res., 64,* 2129-2133.

Haurwitz, B. (1951), The Perturbation Equations in Meteorology, *Compendium of Meteorlogy, (American Met. Soc., Boston),* 401.

Hawkins, G. S. (1963), The Harvard Radio Meteor Project, Proc. of the Symposium on the Astronomy and Physics of Meteors, *Smith Contr. Astrophys., 7*, Washington, D. C.

Hines, C. O. (1960), Internal Atmospheric Gravity Waves at Ionospheric Heights, *Can. J. Phys., 38*, 1441-1481.

Hines, C. O. (1963), Upper Atmosphere in Motion, *Quar. J. Roy. Met. Soc., 89*, 1-42.

Lee, W. and M. A. Geller (1973), Preliminary Design Study of a High-Resolution Meteor Radar, *Aeron. Rep. 52*, Aeron. Lab., Dep. Elec. Eng., Univ. Ill., Urbana-Champaign.

Lindzen, R. S. (1969), Data Necessary for the Detection and Description of Tides and Gravity Waves in the Upper Atmosphere, *J. Atmos. Terr. Phys., 31*, 449-456.

Manning, L. A., O. G. Villard, Jr. and A. M. Peterson (1950), Meteoric Echo Study of Upper Atmopshere Winds, *Proc. IEEE, 47*, 186-199.

Minzner, R. A., K. S. W. Champion and H. L. Pond (1959), The ARDC Model Atmopshere 1959, *Geophys. Survey 115*, ARCBC, Bedford, Mass.

Mitra, S. K. (1949), A Radio Method of Measuring Winds in the Ionosphere, *Proc. IEEE, 43*, 441-446.

Rosenberg, N. W. (1968), Statistical Analysis of Ionospheric Winds - II, *J. Atmos. Terr. Phys., 30*, 907-917.

Rosenberg, N. W., and S. Zimmerman (1972), Ionospheric Winds and Viscous Dissipation, *Radio Sci., 7*, 377-380.

Witt, G. (1962), Height, Structure, and Displacement of Noctilucent Clouds, *Tellus, 14*, 1-18.

APPENDIX I

PRINCIPLE OF DOPPLER DETERMINATION

Measure the quantities M_1, M_2, M_3, defined as

$$M_1 = A \cos(\theta + \omega t_1)$$

$$M_2 = A \sin(\theta + \omega t_2)$$

$$M_3 = A \cos(\theta + \omega t_3)$$

θ = phase angle.

ω = Doppler frequency.

A = Scale factor corresponding to the amplitude of the echo.

The three measurements are taken sequentially, with the time between measurements given by the pulse repetition period Δt; therefore

$$t_2 - t_1 = t_3 - t_2 = \Delta t$$

The three measurements are then rewritten

$$M_1 = A \cos(\theta + \omega t_2 - \omega \Delta t)$$

$$M_2 = A \sin(\theta + \omega t_2)$$

$$M_3 = A \cos(\theta + \omega t_2 + \omega \Delta t)$$

Let $\beta = \theta + \omega t_2$

$\alpha = \omega \Delta t$

Then $M_1 = A \cos(\beta - \alpha)$

$M_2 = A \sin\beta$

$M_3 = A \cos(\beta + \alpha)$

Also $M_1 = A \cos\beta \cos\alpha + A \sin\beta \sin\alpha$

$M_3 = A \cos\beta \cos\alpha - A \sin\beta \sin\alpha$

Combine the three measurements as follows:

$$\frac{M_1 - M_3}{2\,M_2} = \frac{2\,A\,\sin\beta\,\sin\alpha}{2\,A\,\sin\beta}$$

$$= \sin\alpha$$

$$= \sin\,\omega\Delta t$$

$$\omega\Delta t = \sin^{-1}\left[\frac{M_1 - M_3}{2\,M_2}\right]$$

$$\omega = \frac{1}{\Delta t}\,\sin^{-1}\left[\frac{M_1 - M_3}{2\,M_2}\right]$$

APPENDIX II

QUANTIZATION ERROR IN DOPPLER ANGLE DETERMINATION

Let
$$M_1 + \varepsilon_1 = A\cos(\beta - \alpha)$$
$$M_2 + \varepsilon_2 = A\sin\beta$$
$$M_3 + \varepsilon_3 = A\cos(\beta + \alpha)$$

ε_i, $i = 1, 3$ are truncation errors due to A/D conversion.

$$0 \le \varepsilon_i < 1$$

Let
$$Z' = \frac{M_1 - M_3}{2M_2} \quad \text{for } M_2 \neq 0$$

$$= \frac{2A\sin\beta\sin\alpha - \varepsilon_1 + \varepsilon_3}{2(A\sin\beta - \varepsilon_2)}$$

$$= \frac{\sin\alpha - \dfrac{\varepsilon_1 - \varepsilon_3}{2(M_2 + \varepsilon_2)}}{1 - \dfrac{\varepsilon_2}{M_2 + \varepsilon_2}}$$

Since $M_2 \neq 0$, $\dfrac{\varepsilon_2}{M_2 + \varepsilon_2} \neq 1$. Then the expression for Z' can be expanded

$$Z' = \left[\sin\alpha + \frac{\varepsilon_3 - \varepsilon_1}{2(M_2 + \varepsilon_2)}\right]\left[1 + \frac{\varepsilon_2}{M_2 + \varepsilon_2} + \text{higher order terms}\right]$$

$$Z' \cong \sin\alpha + \frac{1}{M_2 + \varepsilon_2}\left[\frac{\varepsilon_3 - \varepsilon_1}{2} + \varepsilon_2\sin\alpha\right]$$

The error in Z' is defined as

$$\Delta Z' = Z' - \sin\alpha$$

Then if values for ε_1, ε_2, and ε_3 are chosen such that the error is maximized, an upper bound on the error in Z' is found.

$$|\Delta Z'| \leq \left| \frac{1/2 + \sin|\alpha|}{M_2} \right|$$

APPENDIX III

THE PESSIMUM CONDITION FOR DOPPLER DETERMINATION

$$M_2 = A \sin(\theta + \omega t_2)$$

$$M_3 = A \cos(\theta + \omega t_3)$$

Let $\phi = \theta + \omega t_2$

$\alpha = \omega(t_3 - t_2)$

Then $M_2 = A \sin \phi$

$M_3 = A \cos(\phi + \alpha)$

Given α, find the lowest magnitude that the higher of the two measurements M_2 and M_3 can reach for arbitrary values of ϕ. The pessimum condition is that $|M_2| = |M_3|$.

Assume $|M_2| = |M_3|$

$$|A \sin\phi| = |A \cos(\phi + \alpha)|$$

$$|\sin\phi| = \left|\sin(\pm \frac{n\pi}{2} + \phi + \alpha)\right| \quad n = 1, 3, 5, \ldots$$

$$\pm\phi = (\pm \frac{n\pi}{2} + \phi + \alpha)$$

There are four solutions:

(1) $$\phi = \pm \frac{n\pi}{2} + \phi + \alpha$$

$$\alpha = \mp \frac{n\pi}{2}$$

(2) $$-\phi = \pm \frac{n\pi}{2} + \phi + \alpha$$

$$\phi = \mp \frac{n\pi}{4} - \frac{\alpha}{2}$$

(3) $$\phi = \mp \frac{n\pi}{2} - \phi - \alpha$$

$$\phi = \mp \frac{n\pi}{4} - \frac{\alpha}{2}$$

(4) $$-\phi + \mp \frac{n\pi}{2} - \phi - \alpha$$

$$\alpha = \pm \frac{n\pi}{2}$$

Cases (1) and (4), where $\alpha = \pm \frac{n\pi}{2}$, imply that the minimum of M_2 or M_3 is zero. Cases (2) and (3) are the required solutions for $-\pi/2 < \alpha < \pi/2$. Cases (2) and (3) can be combined

$$\phi = \pm \frac{n\pi}{4} - \left|\frac{\alpha}{2}\right| \qquad n = 1, 3, \ldots$$

Then the pessimum condition gives that

(a) $$\left|M_2\right| = \left|A \sin\left(\frac{\pi}{4} - \left|\frac{\alpha}{2}\right|\right)\right|$$

or

(b) $$\left|M_2\right| = \left|A \sin\left(\frac{3\pi}{4} - \left|\frac{\alpha}{2}\right|\right)\right|$$

Consider case (a) only. Case(a) is the pessimum condition for $-\pi/2 < \alpha < \pi/2$: case (b) is the condition for $\pi < |\alpha| < \pi/2$, which is not of interest. Then the lowest magnitude that the higher of $|M_2|$ or $|M_3|$ can have is

$$\text{Max}\left|M_2, M_3\right| \geq \left|A \sin\left(\frac{\pi}{4} - \frac{|\alpha|}{2}\right)\right|$$

APPENDIX IV

INTERFEROMETER PHASE DIFFERENCE DETERMINATION

Measure at time

t_1: $M_1 = A_1 \sin(\phi_1 + \omega t_1)$

t_2: $M_2 = A_1 \cos(\phi_1 + \omega t_2)$ from Antenna #1

t_3: $M_3 = A_2 \sin(\phi_2 + \omega t_3)$

t_4: $M_4 = A_2 \cos(\phi_2 + \omega t_4)$ from Antenna #2

Let

$$\omega t_1 = \theta_A$$
$$\omega t_2 = \theta_B$$
$$\omega t_3 = \theta_C$$
$$\omega t_4 = \theta_D$$

Then

$$M_1 = A_1 \sin(\phi_1 + \theta_A)$$
$$= A_1 \sin\phi_1 \cos\theta_A + A_1 \cos\phi_1 \sin\theta_A$$

$$M_2 = A_1 \cos(\phi_1 + \theta_B)$$
$$= A_1 \cos\phi_1 \cos\theta_B - A_1 \sin\phi_1 \sin\theta_B$$

$$M_3 = A_2 \sin(\phi_2 + \theta_C)$$
$$= A_2 \sin\phi_2 \cos\theta_C + A_2 \cos\phi_2 \sin\theta_C$$

$$M_4 = A_2 \cos(\phi_2 + \theta_D)$$
$$= A_2 \cos\phi_2 \cos\theta_D - A_2 \sin\phi_2 \sin\theta_D$$

$$A_1 \sin\phi_1 = \frac{M_1 \cos\theta_B - M_2 \sin\theta_A}{\cos(\theta_A - \theta_B)}$$

$$A_1 \cos\phi_1 = \frac{M_2 \cos\theta_A + M_1 \sin\theta_B}{\cos(\theta_A - \theta_B)}$$

$$A_2 \sin\phi_2 = \frac{M_3 \cos\theta_D - M_4 \sin\theta_C}{\cos(\theta_C - \theta_D)}$$

$$A_2 \cos\phi_2 = \frac{M_4 \cos\theta_C + M_3 \sin\theta_D}{\cos(\theta_C - \theta_D)}$$

Let $X = A_1 A_2 \cos(\phi_1 - \phi_2) \cos(\theta_A - \theta_B) \cos(\theta_C - \theta_D)$

$$Y = A_1 A_2 \sin(\phi_1 - \phi_2) \cos(\theta_A - \theta_B) \cos(\theta_C - \theta_D)$$

$$X = [A_1 \cos\phi_1 A_2 \cos\phi_2 + A_1 \sin\phi_1 A_2 \sin\phi_2] \cos(\theta_A - \theta_B) \cos(\theta_C - \theta_D)$$
$$= [M_1 \sin\theta_B + M_2 \cos\theta_A][M_3 \sin\theta_D + M_4 \cos\theta_C]$$
$$+ [M_1 \cos\theta_B - M_2 \sin\theta_A][M_3 \cos\theta_D - M_4 \sin\theta_C]$$

$$X = M_1 M_3 \cos(\theta_B - \theta_D) + M_1 M_4 \sin(\theta_B - \theta_C) - M_2 M_3 \sin(\theta_A - \theta_D)$$
$$+ M_2 M_4 \cos(\theta_A - \theta_C)$$

$$Y = [A_1 \sin\phi_1 A_2 \cos\phi_2 - A_1 \cos\Phi_1 A_2 \sin\phi_2] \cos(\theta_A - \theta_B) \cos(\theta_C - \theta_D)$$
$$= [M_1 \cos\theta_B - M_2 \sin\theta_A][M_3 \sin\theta_D + M_4 \cos\theta_C]$$
$$- [M_3 \cos\theta_D - M_4 \sin\theta_C][M_1 \sin\theta_B + M_2 \cos\theta_A]$$

$$Y = M_1 M_4 \cos(\theta_B - \theta_C) - M_2 M_3 \cos(\theta_A - \theta_D) - M_1 M_3 \sin(\theta_B - \theta_D)$$
$$- M_2 M_4 \sin(\theta_A - \theta_C)$$

If $\theta_D - \theta_C = \theta_C - \theta_B = \theta_B - \theta_A = \omega\Delta t$

and $\omega\Delta t = \alpha$

$$X = (M_1M_3 + M_2M_3)\cos 2\alpha - M_1M_4 \sin\alpha + M_2M_3 \sin 3\alpha$$

$$Y = (M_1M_3 + M_2M_4)\sin 2\alpha + M_1M_4 \cos\alpha - M_2M_3 \cos 3\alpha$$

From the definitions of X and Y,

$$X^2 + Y^2 = A_1^2 A_2^2 \cos^2(\theta_A - \theta_B) \cos^2(\theta_C - \theta_D)$$

Thus

$$\sin(\phi_1 - \phi_2) = \frac{Y}{\sqrt{X^2 + Y^2}}$$

$$\cos(\phi_1 - \phi_2) = \frac{X}{\sqrt{X^2 + Y^2}}$$

Note that these ratios are singular only when $\cos\alpha = 0$.

APPENDIX V

METEOR RADAR PROGRAMS

```
C.   BACKOF
C    EDIT #14 MOD2
C    TRY4 IS A PROGRAM TO SIMULATE THE DATA FROM THE METEOR
C    TRAIL SEARCH AND STORE PROGRAM.  IT TAKES AS INPUT DATA
C    THE SYSTEM DESCRIPTION AND THE COORDINATES AND VELOCITY
C    OF REFLECTION POINTS.  ALSO THE NUMBER OF ITERATIONS IS
C    INPUT.  THE INITIAL PHASE IS ROTATED BY 2PI/N RADIANS FOR
C    EACH TEST, WHERE N IS THE NUMBER OF ITERATIONS.  THE RES-
C    ULTS OF EACH TEST ARE AVERAGED, AND ONLY THE AVERAGE AND
C    STANDARD DEVIATION ARE PRINTED.  THIS TEST DOES NOT IN-
C    CLUDE THE RANGE ALGORITHM.
C
C    APRIL 19 1973
C
C   GET SYSTEM DESCRIPTION
C
         DIMENSION N(16),AN(16),K(32)
         WRITE(6,1)
1        FORMAT(1H1,22X,28HT R Y O U T  FRAME GENERATOR ///
         11H ,27X,18HSYSTEM DESCRIPTION //17H AZIMUTH SPACING: )
         CALL FFIR(1,AZSP)
2        FORMAT(F10.5)
         WRITE(6,3)
3        FORMAT(//24H FINE ELEVATION SPACING: )
         CALL FFIR(1,FELSP)
         WRITE(6,4)
4        FORMAT(//26H COARSE ELEVATION SPACING: )
         CALL FFIR(1,CELSP)
         INT=9287
C
C    ASK FOR PARTICULARS OF EACH METEOR
C
5        WRITE(6,6)
6        FORMAT(38H ************************************
         1/21H AMPLITUDE(1 TO 500): )
         CALL FFIR(1,A)
         WRITE(6,7)
7        FORMAT(17H NOISE STAND.DEV. )
         CALL FFIR(1,SD)
         WRITE(6,8)
8        FORMAT(22H ELEVATION ANGLE (RAD) )
         CALL FFIR(1,EL)
         WRITE(6,9)
9        FORMAT(28H ANGLE WITH DUE NORTH (RAD): )
         CALL FFIR(1,AZ)
         WRITE(6,10)
10       FORMAT(23H RADIAL VELOCITY (M/S)    )
         SUMAZ=0.
         SUMEL=0.
         SUMVL=0.
```

```
      SSQAZ=0.
      SSQEL=0.
      SSQVL=0.
      CALL FFIR(1,V)
      WRITE(6,13)
13    FORMAT( 18H NO. OF ITERATIONS )
C
CALCULATIONS
C
      WDT=V/233.2036
      CALL FFIR(1,QU)
      IQ=QU
      CSEL=COS(EL)
      FELD=-6.2832*FELSP*CSEL*COS(AZ)
      CELD=6.2832*CELSP*CSEL*COS(AZ)
      AZD=-6.2832*AZSP*CSEL*SIN(AZ)
      DO 100 II=1,IQ
      PH=6.2832/QU*FLOAT(II)
      DO 15 I=2,5
15    AN(I)=PH
C  ANGLES AT ANTENNAS
C
      DO 17 I=6,9
17    AN(I)=PH+FELD
      AN(1)=0.
      AN(10)=0.
      AN(11)=PH+CELD
      AN(12)=AN(11)
      AN(13)=PH
      AN(14)=PH
      AN(15)=PH+AZD
      AN(16)=AN(15)
C
C    PUT IN DOPPLER FREQUENCY CHANGE
      DO 20 I=1,16
      AN(I)=AN(I)+WDT*FLOAT(I)
20    AN(I)=AMOD(AN(I),6.2832)
      DO 30 I=2,9,2
30    N(I)=A*SIN(AN(I))+GAUSS(INT)*SD
      DO 40 I=3,9,2
40    N(I)=A*COS(AN(I))+GAUSS(INT)*SD
      DO 50 I=11,16,2
50    N(I)=A*SIN(AN(I))+GAUSS(INT)*SD
      DO 60 I=12,16,2
60    N(I)=A*COS(AN(I))+GAUSS(INT)*SD
      N(1)=R@D/3.+.5
      N(10)=N(1)
      CALL SDRIVI(N,AZ,EL,VEL)
      SUMAZ=SUMAZ+AZ
      SUMEL=SUMEL+EL
      SUMVL=SUMVL+VEL
      SSQAZ=SSQAZ+AZ*AZ
```

```
      SSQEL = SSQEL+EL* EL
100   SSQVL = SSQVL+VEL* VEL
      AVAZ=SUMAZ/QU
      AVEL=SUMEL/QU
      AVVL=SUMVL/QU
      SDAZ=SQRT((SSQAZ-SUMAZ* SUMAZ/QU) /(QU-1.))
      SDEL=SQRT((SSQEL-SUMEL* SUMEL/QU) /(QU-1.))
      SDVL=SQRT((SSQVL-SUMVL* SUMVL/QU) /(QU-1.))
      WRITE(6,200)AVQZ,SDAZ,AVEL,SDEL,AVVL,SDVL
200   FORMAT(12X,7HAVERAGE,6X,12HSTANDARD DEV/
     1         10H AZIMUTH  ,F9.4,7X,F8.4/
     2         10H ELEVQTION,F9.4,7X,F8.4/
     3         10H VELOCITY ,F9.4,7X,F8.4)
      GOTO 5
      END
```

```
      BLOCK DATA
C.  BACKOF
C   EDIT #1
C   ERROR INITIALIZES IERR TO ZERO...  THAT'S ALL!
      COMMON /ERROR/ IERR
      DATA IERR/0/
      END


      BLOCK DATA
C. BACKOF
C   EDIT #1
C   JULY 19,1973
C   SPCING IS THE PROGRAM WITH THE ANTENNA SPACING DATA
C
      COMMON /DIST/ AZSP,CELSP,FELSP,R2PI,RPI,RR2PI
C
C   THESE ARE THE RECIPROCLS OF 2PI*ANTENNA SPACINGS
C
      DATA AZSP,CELSP,FELSP/.1591549,.1591549,7.957745E-3/
C
C   THESE ARE 1/FELSP,1/2/FELSP,FELSP
C
      DATA R2PI,RPI,RR2PI/.05,.025,20./
      END

      SUBROUTINE ANGLES(N1,N2,N3,N4,ANGLE)
C. BACKOF 9 MARCH 73
C   EDIT #11
C  SUBROUTINE ANGLES TAKES INFO FROM THE SINE AND COSINE
CHANNELS OF TWO RECEIVERS AND GIVES THE SINE AND COSINE OF THE
C   PHASE DIFFERENCE
      COMMON /TRIG/ SIN1,SIN2,SIN3,COS1,COS2,COS3,ALPHA
      COMMON /ERROR/ IERR
C
CALCULATE FLOATED VALUES
C
      A1=FLOAT(N1)
      A2=FLOAT(N2)
      A3=FLOAT(N3)
      A4=FLOAT(N4)
C
CALCULATE INTERMEDIATE QUANTITIES
C
      Q1=A1*A4
      Q2=A1*A3+A2*A4
      Q3=A2*A3
C
CALCULATE UNNORMALIZED SINE AND COSINE
C
      COS=Q2*COS2-Q1*SIN1+Q3*SIN3
      SIN=Q2*SIN2+Q1*COS1-Q3*COS3
```

```
C
C TDST FOR ERROR CONDITION
C
      IF( SIN .EQ. 0. .AND. COS .EQ. 0. )  GOTO 1
C
CALCULATD ANGLE
C
      ANGLE=TRGINV(SIN,COS)
      IF( ANGLE .LT. 0. )  ANGLE=ANGLE+6.2832
C
C  EXIT TO CALLING ROUTINE
C
      RETURN
C
C ERROR EXIT
C
1     IERR=11
      RETURN
      END

      SUBROUTINE ARRIVL
C. BACKOF   28 MARCH 73
C EDIT #11
C   SUB. ARRIVL TAKES PHASE DIFFS AND ANTENNA SPACINGS, AND
C  RETURNS ANGLES OF ARRIVAL
C
C  SET UP ANTENNA SEPERATION DATA
C
      COMMON /DIST/DAZ,DCEL,DFEL,R2PI,RPI,RR2PI
      COMMON /AOFA/OAZ,OCEL,OFEL,AZANG,ELANG
      COMMON /ERROR/ IERR
C
C    NORMALIZE PHASE
C
      PHAZ=OAZ*DAZ
      IF( PHAZ .GT. .5 ) PHAZ=PHAZ-1.
      PHCEL=OCEL*DCEL
      PHFEL=OFEL*DFEL
C
COMBINE COARSE AND FINE ELEVATION
C
      PHEL=PHFEL+R2PI*AINT(PHCEL*RR2PI)
C
CORRECT
C
      ERR=PHEL-PHCEL
      IF( ERR .LT. -RPI )  PHEL=PHEL+R2PI
      IF( ERR .GT.  RPI )  PHEL=PHEL-R2PI
C
CALC SUM OF PHASES SQUARED
C
      CELSQ=PHEL*PHEL+PHAZ*PHAZ
```

```
C
CALC TRIG
C
      IF( CELSQ .EQ. .0)  GO TO 1
      CEL=SQRT(CELSQ)
      IF( CELSQ .GT. 1. )  GO TO 2
      SEL=SQRT(1.-CELSQ)
C
CHANGE TO ANGLES
C
      AZANG=TRGINV(PHAZ,PHEL)
      ELANG=TRGINV(SEL,CEL)
C
C  EXIT
C
      RETURN
C
C  ERROR EXIT
C
1     IERR=31
      RETURN
2     IERR=32
      RETURN
      END

      FUNCTION DOPPLR(N1,N2,N3,N4)
C. BACKOF 9 MARCH 73
C  EDIT #2
C   FUNCTION DOPPLR TAKES 4 SEQUENTIAL VALUES AND CALCULATES
C   SIN OF THE DOPPLER ANGLE ALPHA
C
C   DEFINE THE TRANSFORMATION
C
      COMMON /ERROR/ IERR
      CRUNCH(I,J,K)=FLOAT(K-I)/FLOAT(J+J)
C
COMPARE MAGNITUDE  OF N2 & N3
C  IF N2 & N3 BOTH ZERO, ERROR EXIT WITH IERR=21,ELSE
CHOOSE THE BETTER METHOD DEPENDING ON THE GREATER MAGNITUDE
C
      MAG2=IABS(N2)
      MAG3=IABS(N3)
      IF( MAG2+MAG3 .EQ. 0 )  GO TO 1
C
CALCULATE DOPPLR
C
      IF( MAG2 .LT. MAG3 )   DOPPLR=CRUNCH(N4,N3,N2)
      IF( MAG2 .GE. MAG3 )   DOPPLR=CRUNCH(N1,N2,N3)
C
C EXIT TO CALLING PROGRAM
C
      RETURN
```

```
C
C ERROR EXIT
C
1       IERR=21
        RETURN
        END

C. BACKOF
C  FEB 22,74
C
C  THIS FUNCTION CALCULATES TAU FOR THE RANGE ALGORITHM
C  USING THE PARABOLA METHOD
C
C  THREE ARGUAMENTS ARE REQUIRED:  THE HIGHEST SAMPLE, AND ITS
C  TWO NEIGHBORS
C
      FUNCTION ITAU(N1,N2,N3)
C
      ITAU=IFIX(5.*FLOAT(N1-N3)/FLOAT(N1+N3-N2-N2)+.5)
C
      RETURN
      END

      SUBROUTINE SDRIV1(N,A1,A2,A3)
C. BACKOF  20 APRIL 73
C  EDIT #11  MOD 2
C
C  SDRIV1 IS THE SUBROUTINE DRIVER.  IT FORMATS DATA AND
C  CALLS THE PROCESSING SUBROUTINES IN THE PROPER ORDER.
C
C  GET SYSTEM DESCRIPTION
C
      DIMENSION N(16)
      COMMON /AOFA/ AZ,CEL,FEL,AZANG,ELANG
      COMMON /TRIG/ S1,S2,S3,C1,C2,C3,ALPHA
      COMMON /ERROR/ IERR
C
C  TST DOPPLER
C
      SDOP1=DOPPLR(N(2),N(3),N(4),N(5))
      IF( IERR .NE. 0 )  GO TO 20
      SDOP2=DOPPLR(N(6),N(7),N(8),N(9))
      IF( IERR .NE. 0 )  GO TO 20
      S1=(SDOP1+SDOP2)/2.
C
C  TST SINCOS  ;  GET SINES & COSINES
C
      CALL SINCOS
      IF( IERR .NE. 0 )  GO TO 20
CALCULATE VELOCITY
C
      VEL=233.2036*ALPHA
```

```
C
C    GET FINE ELEV PHASE DIFFERENCE
C
          CALL ANGLES(N(4),N(5),N(6),N(7),FEL)
          IF( IERR .NE. 0 )  GO TO 20
C
C   GET COARSE EL PHSE DIFF
C
          CALL ANGLES(N(11),N(12),N(13),N(14),CEL)
          IF( IERR .NE. 0 )  GO TO 20
C
C   AZ ANG PHSE DIFF
C
          CALL ANGLES(N(13),N(14),N(15),N(16),AZ)
          IF( IERR .NE. 0 )  GO TO 20
C
C   GET OF ANGLES OF ARRIVAL
C
          CALL ARRIVL
          IF( IERR .NE. 0 )  GO TO 20
          A1=AZANG
          A2=ELANG
          A3=VEL
C
C OUTPUT RESULTS
C
          RETURN
20        WRITE(6,11)  IERR
          IERR=0
11        FORMAT(/3X,8H*** ERROR,I3,3H*** )
          RETURN
          END


          SUBROUTINE SINCOS
C. BACKOF  14 MARCH 73
C      SUBROUTINE SINCOS TAKES SIN OF ALPHA AS INPUT AND RETURNS
C      SIN AND COS OF ALPHA, 2*ALPHA, 3*ALPHA,@ND ALPHA ITSELF
C
          COMMON /TRIG/ SIN1,SIN2,SIN3,COS1,COS2,COS3,ALPHA
C
CALC SIN & COS SQUARED
C
          COMMON /ERROR/ IERR
          SINSQ1=SIN1*SIN1
          COSSQ1=1.-SINSQ1
          IF( COSSQ1 .LT. 0. )  GO TO 1
C
CALC COSINE
C
          COS1=SQRT(COSSQ1)
```

```
C
CALC ALL OTHER QUANTITIES FROM ABOVE RELATIONS
C
      SIN2=2.*SIN1*COS1
      COS2=COSSQ1-SINSQ1
      SIN3=SIN1*(3.*COSSQ1-SINSQ1)
      COS3=COS1*(COSSQ1-3.*SINSQ1)
C
CALCULATE ANGLE
C
      ALPHA=TRGINV(SIN1,COS1)
C
C  EXIT TO CALLING PROGRAM
C
      RETURN
C
C  ERROR EXIT
C
1     IERR=41
      RETURN
      END

      FUNCTION TRGINV(A,B)
C BACKOF 21 JULY 73
C  VERSION EDIT #2
C  FUNCTION TRGINV TAKES 2 V@LUES AND RETURNS THE ARCTAN OF
C  THEIR RATIO
C
CHECK FOR ZERO DENOMINATOR
C
      IF( B .EQ. 0. )  GO TO 1
      TRGINV=ATAN2(A,B)
C
C  EXIT
C
      RETURN
C
C  B=0
C
1     IF( A .GE. 0. ) TRGINV=1.5707963
      IF( A .LT. 0. ) TRGINV=-1.5707963
      RETURN
      END
```

```
/
/ C. BACKOF
/ FEB 27,74
/
/  CLOCK STARTS THE FIRST WORD IN THE COMMON
/ BLOCK 'STATUS' COUNTING SECONDS
/
/ CALLED FROM FORTRAN BY
/    'CALL CLOCK'
/
        .GLOBL  CLOCK,STATUS
CLOCK   0
        DZM*    STATUS          /ZERO AT START
        .TIMER  60,INC,5        /FIRST CALL
        JMP*    CLOCK
INC     0                       /INTERRUPT SERVICE
        DAC     SAVE            /SAVE ACC
        .TIMER  60,INC,5        /RESTART TIMER
        ISZ*    STATUS          /AND COUNT
        LAC     SAVE
        .RLXIT  INC
SAVE    0
        .END

        FUNCTION GAUSS(II)
C   GAUSS GENERATES RAND NUMBS WITH A GAUSSIAN DISTRIBUTION
C   C.  BACKOF
C   AUG 25 73
C
        GAUSS=-6.
        DO 1 I=1,12
1       GAUSS=GAUSS+RANDU(II)
        RETURN
        END

C       FUNCTION TO CALCULATE RANDOM NUMBERS
        FUNCTION RANDU(IR)
        IR=IR*653
        IF(IR.LT.0) IR=IR-1
        IR=IR + 257
        IF(IR.LT.0) IR=IR + 131071 + 1
        RANDU=FLOAT(IR)/131071.0
        RETURN
        END
```

```
C. BACKOF
C   FEB 27,74
C
C   METEOR ECHO SEARCH
C
C   FIRST, THE NAME
C
          SUBROUTINE SRCH
C
C   AND PRELIMINARIES
C
          COMMON /STATUS/ ITIM,ILIN,IFRM,ITOP,IBOT
          COMMON /FRAME/ I(3200)
          COMMON /STACK/ J(223)
          DATA ITH/100/
C
C   FIGURE OUT WHICH FRAME TO SEARCH
C
          IS=2
          IF( IFRM .EQ. 0 )  IS=1602
          IE=IS+98
C
C   TEST FOR BAD FRAME
C   (IF FIRST WORD IS -1)
C
          IF(I(IS-1) .EQ. -1)  GOTO 4
C
C   SEARCH FIRST RANGE LINE FOR MAX
C
          MAX=0
1         K=I(IS)
          IF( K.LT.MAX .OR. K.GT.511 )  GOTO 2
          MAX=K
          IP=IS
2         IS=IS+1
          IF( IS .NE. IE )  GOTO 1
C
C   MAX IS THE VALUE OF THE MAX, IP ITS POSITION
C   GET CORRESPONDING ELEMENT FROM OTHER RANGE
C   LINE;  GET RID OF CHANNEL ID
C
          MAX2=I(IP+900)+114688
C
C   AND TEST FOR THRESHOLD
C
          IF( MAX.GT.ITH .AND. MAX2 .GT.ITH )  GOTO 3
C
C THRESHOLD TEST FAILED
C
          RETURN
```

```
C
C   BUILD REDUCED FRAME
C
3       K=ITOP*22+1
C
C   K IS THE FIRST WORD OF THE TOP LINE ON THE STACK
C
        IF( J(K).NE.0 )  GOTO 4
C
C   STACK FULL
C
        J(K)=IP+100-IE
        J(K+1)=I(IP-1)
        J(K+2)=MAX
        J(K+3)=I(IP+1)
        J(K+4)=I(IP+899)
        J(K+5)=I(IP+900)
        J(K+6)=I(IP+901)
        J(K+7)=I(IP+100)
        J(K+8)=I(IP+200)
        J(K+9)=I(IP+300)
        J(K+10)=I(IP+400)
        J(K+11)=I(IP+500)
        J(K+12)=I(IP+600)
        J(K+13)=I(IP+700)
        J(K+14)=I(IP+800)
        J(K+15)=I(IP+1000)
        J(K+16)=I(IP+1100)
        J(K+17)=I(IP+1200)
        J(K+18)=I(IP+1300)
        J(K+19)=I(IP+1400)
        J(K+20)=I(IP+1500)
        J(K+21)=ITIM
C
C REDUCED FRAME IS ON STACK
C  UPDATE TOP OF STACK
C
        ITOP=ITOP+1
        IF( ITOP.GE.10 )  ITOP=0
C
C   AND LEAVE
C
4       I(IE-99)=0
        RETURN
        END

/
/C. BACKOF
/ FEB 28,74
/
/THIS IS THE ASSEMBLY PORTION OF
/THE COLLECTION AND R@NGE SEARCH SUBSYSTEMS
/TO START, USE THE FORTRAN STATEMENT
/    'CALL ADC'
```

```
/
        .GLOBL STATUS,FRAME,ADC
ADC     0
        LAC*    (155            /.SETUP ROUTINE
        DAC     HOLD
        JMS*    HOLD            /GO TO IT
        703701                  /SKIP INSTRUCTION
        INT                     /INT SVC ROUTINE
/
/ INDICATE FIRST FRAME BAD
/
        LAW     -1
        DAC*    FRAME
/
/FIRST CALL FOR INPUT
/
        LAW     -144            /100(DEC) WORDS
        DAC*    (26             /TO WORD COUNT
        LAC     FRAME           /FRAME +100
        TAD     (144            /IS 2ND LINE
        DAC     START           /FIRST  BUFF
        TAD     (-1
        DAC*    (27             /TO DATA CHAN ADDR
/
/   FIX UP ADDRESSES OF STATUS WORDS
/
        LAC     STATUS
        IAC
        DAC     LINE
        IAC
        DAC     FRM
/
/   START COLLECTION AND EXIT
/
        703724          /AD WRITE INIT
        JMP*    ADC
/
/    INTERRUPT SERVICE ROUTINE
/
INT     0
/
/   SAVE REGISTERS
/
        DAC     SAVAC
        LACQ
        DAC     SAVMQ
        GLK
/
/   TEST FOR ERROR
/
        703721                  /SKIP ON AD ERROR
        JMP     OVER
```

```
        LAC*    FRM
        SZA
        .DEC
        LAC     (1600
        .OCT
        TAD     FRAME
        DAC     HOLD
        LAW     -1              /ERROR FLAG TO 1 ST
        DAC*    HOLD            /WORD  OF FRAME
/
/FIGURE OUT WHICH CHANNEL WAS COLLECTED
/
OVER    LAC*    START           /GET FIRST SAMPLE
        CLL                     /SHIFT 14(DEC) RIGHT
        LRS     16
        IAC                     /+1
        DAC     CHAN            /CHANNEL ID
        TAD     (-20            /EQUAL 16(DEC)?
        SZA
        JMP     DOWN            /NO
/
/  FRAME JUST FILLED
/
        LAC*    FRM             /COMPLEMENTT
        SZA!IAC                 /FRAME POINTER
        CLA
        DAC*    FRM
        DZM     CHAN            /BACK TO CHAN 0
        .TIMER  0,RNG,6         /START RANGE SEARCH
/
/  FIGURE THE START OF THE NEXT BUFFER
/
DOWN    LAC*    FRM             FRAME POINT
        SZA
        LAC     (20             /TIMES 16(DEC)
        ADD     CHAN
        DAC*    LINE            /NEXT LINE
        MUL
        144                     /TIMES 100(DEC
        LACQ
        TAD     FRAME
        DAC     START           /START OF BUFFER
/
/ NOW SET UP TRANSFER
/
        TAD     (-1
        DAC*    (27             /BUFF ADDR
        LAW     -144            /WORD COUNT
        DAC*    (26
```

```
/
/RESET REGISTERS
/
        RAR
        LAC     SAVMQ
        LMQ
        LAC     SAVAC
/
/  AND EXIT
/
        703724                  /ENABLE COLLECT
        DBR                     /LEAVE API0
        JMP*    INT             /EXIT
/
/  CALL TO FORTRAN RANGE SEARCH
/
RNG     0
        JMS*    SRCH
        .RLXIT  RNG
/
/ STORAGE AREA
/
LINE    0
FRM     0
HOLD    0
SAVAC   0
SAVMQ   0
START   0
CHAN    0
        .END
```